Paleoceanography and Paleoclimatology

RESEARCH ARTICLE
10.1029/2020PA004009

The Postglacial Isotopic Record of Intermediate Water Connects Mediterranean Sapropels and Organic-Rich Layers

Alessandro Incarbona[1] and Mario Sprovieri[2]

[1]Dipartimento di Scienze della Terra e del Mare, Università di Palermo, Sicily, Italy, [2]Istituto per lo Studio degli Impatti Antropici e Sostenibilità in Ambiente Marino, Consiglio Nazionale delle Ricerche, Genoa, Italy

Key Points:

- LIW density decreases and reduced seafloor ventilation are recorded coinciding with the sapropel onset and the maximum Nile River flooding
- A denser LIW and higher seafloor ventilation correspond with the final TOC accumulation in the western Mediterranean that marks the ORL end
- Eastern Mediterranean perturbations were transmitted into the western Mediterranean through the zonal vertical circulation belt

Correspondence to:
A. Incarbona,
alessandro.incarbona@unipa.it

Citation:
Incarbona, A., & Sprovieri, M. (2020). The postglacial isotopic record of intermediate water connects Mediterranean sapropels and organic-rich layers. *Paleoceanography and Paleoclimatology*, *35*, e2020PA004009. https://doi.org/10.1029/2020PA004009

Received 16 MAR 2020
Accepted 19 AUG 2020
Accepted article online 9 SEP 2020

Abstract Carbon-rich layers exist at both sides of the Mediterranean Sea sedimentary record and are called sapropels and organic rich layers (ORLs), respectively, in the eastern and western basins. They have different levels of organic carbon accumulation and seafloor oxygen deprivation. The most recent sapropel and ORL depositions have a different timing, approximately 10.8–6.1 and 14.5–9.0 ka, respectively. Here we investigate oxygen isotopic records of three foraminifera species that occupy different habitats within the Sicily Channel water column since ~12.0 ka, thus in the sill between the eastern and western Mediterranean basins. These data are ice volume corrected, to get information on water masses density variability, and are accompanied by benthic foraminifera $\delta^{13}C$ measurements to establish Sicily Channel seafloor ventilation. Our results, and the comparison with other chronologically well-constrained Mediterranean records, highlight the connection of the two subbasins due to monsoon activity. The end of the maximum Nile River flooding at ~9.2 ka, and eastern Mediterranean seafloor reventilation above 1,800–1,500 m depth at ~ 8.2 and 7.2 ka, left a clear signature in the intermediate water isotopic record of the Sicily Channel. Concurrently, the western Mediterranean deep water circulation experienced a significant recovery after a long period of slowdown. We argue that African monsoon weakening was transmitted into the western Mediterranean, through the intermediate layer of circulation, where deep water formation took place and brought oxygen to the seafloor.

1. Introduction

The Mediterranean Sea thermohaline circulation reproduces global ocean processes, in terms of deep water formation processes and of climate-driven thermohaline circulation (Bethoux et al., 1999), and can schematically be subdivided into three meridional and zonal circulation cells. The zonal vertical circulation belt deals with surface Atlantic water (Modified Atlantic Water, MAW) and its transformation into intermediate water (Levantine Intermediate Water, LIW) (Figure 1a). Meridional cells are driven by deep water formation in the Gulf of Lions and in the Adriatic Sea (Pinardi & Masetti, 2000) (Figure 1a). Deep water formation is preconditioned by LIW that contributes to the vertical advection (Wu & Haines, 1996). This means that zonal and meridional cells are interconnected and the eastern and western Mediterranean overturning cells can communicate with each other through the zonal cell (Pinardi & Masetti, 2000).

In the late 1980s and early 1990s, a saltier and warmer intermediate water led to enhanced deep water production in the Aegean Sea that replaced the one from the Adriatic Sea, the so-called Eastern Mediterranean Transient (EMT) (Roether et al., 1996). In less than 2 years (2004–2006) the whole western Mediterranean basin has been filled by a new highly saline and warm deep water (Schroeder et al., 2008). Models and observations claim the major role of salty intermediate water, exported from the eastern Mediterranean after the EMT, for preconditioning the upper 1,000 m of the Gulf of Lions water column and for vertical advection (Schroeder et al., 2010; Skliris & Lascaratos, 2004). Such a phenomenon demonstrates that today's local oceanographic perturbations are rapidly transmitted across the whole basin. The same coordinated response of the two subbasins remains poorly understood for the thermohaline circulation variability due to changes in climate in the last tens of thousands of years.

Eastern Mediterranean sapropels are thought to be the result of eccentricity modulation of precession minima (Hilgen, 1991; Lourens et al., 1997) that enhanced monsoon activity and freshwater discharge from North African rivers (Hennekam et al., 2014; Marino et al., 2009; Rohling, Cane, et al., 2002; Rossignol-Strick

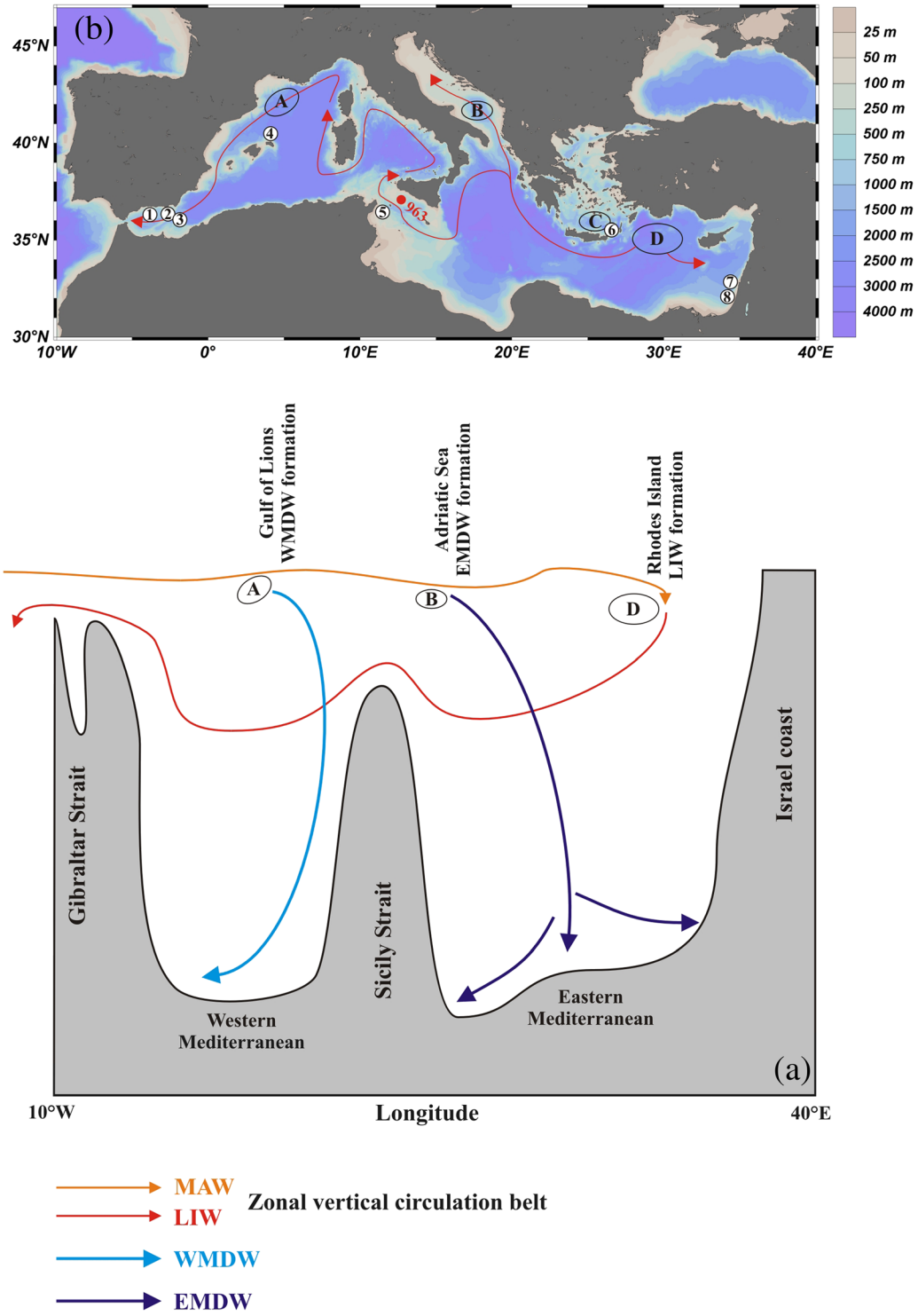

Figure 1. (a) Schematic plot of Mediterranean Sea circulation. (b) Mediterranean Sea bathymetry and location of the cores discussed in the text. The red arrow indicates the main path of LIW (modified from Pinardi & Masetti, 2000). The red circle indicates the location of ODP Hole 963D. (a) Gulf of Lions deep water formation site. (b) Adriatic Sea deep water formation site. (c) Aegean Sea deep water formation site. (d) LIW formation site. With numbered circles indicate the location of cores discussed in the manuscript. (1) ODP Site 976 (Martrat et al., 2014). (2) MD95-2043 (Cacho et al., 1999, 2000, 2002, Martrat et al., 2004, 2014). (3) ODP Site 977 (Martrat et al., 2004, 2014). (4) MD99-2343 (Frigola et al., 2008). (5) MD04-2797CQ (Bout-Roumazeilles et al., 2013). (6) LC21 (Abu-Zied et al., 2008; Casford et al., 2003; Marino et al., 2009). (7) SL112 (Weldeab et al., 2014). (8) PS009PC (Hennekam et al., 2014).

et al., 1982; Weldeab et al., 2014). Enhanced productivity and preservation are the common explanations for distinctive organic carbon beds (Rohling et al., 2015) and imply oceanographic processes (e.g., nutricline shoaling within the photic zone, cessation of deep water formation, and seafloor anoxia) that have necessarily involved awesome modifications in the intermediate water layer of the thermohaline circulation (Grimm et al., 2015; Rogerson et al., 2008; Zirks et al., 2019). On the other hand, western Mediterranean organic rich layers (ORLs) are associated with enhanced productivity and reduced deep ventilation that led to seafloor dysoxia (Rogerson et al., 2008). Most of ORLs are expected to be deposited at the same time as eastern Mediterranean sapropels, because LIW may convey eastern Mediterranean salinity reduction into the western Mediterranean (Emeis et al., 1991; Rohling et al., 2015). However, the most recent sapropel and ORL were deposited in different time intervals (Cacho et al., 2002), denoting the action of different forcing or the presence of local perturbations, like the discharge of alpine meltwater in the western Mediterranean (Rogerson et al., 2008; Rohling et al., 2015).

Here we investigate high-resolution (~100 years on average) stable isotope records (planktonic and benthic foraminifera $\delta^{18}O$ and benthic foraminifera $\delta^{13}C$) since the late Younger Dryas in the Sicily Channel, whose seafloor is placed at the depth of about 470 m and is directly crossed by LIW in transit to the Tyrrhenian Sea (Figure 1A). We examine different species that thrive surface MAW, upper LIW, and core LIW. Oxygen isotopes are ice volume corrected for understanding how LIW density variability may have affected western Mediterranean vertical advection, while diachronous sapropel S1 and the most recent ORL were being deposited. The paper is aimed at assessing postglacial LIW density variability and Sicily Channel seafloor ventilation changes. This information is used to find any potential signal that connects the eastern and the western Mediterranean, by comparison with high-resolution and well-constrained records from the Aegean, Levantine, and the Alboran Seas.

2. Material and Methods

The Ocean Drilling program (ODP) Hole 963D (longitude 37°02.148′N, latitude 13°10.686′E; 469.1 m below sea level) was recovered in the southern Sicily offshore (Figure 1b). The bulk sediment composition is made up of 8.40 m of brown and greenish nannofossil clay, with rare pyrite (Emeis et al., 1996) and common terrigenous detrital matter (Böttcher et al., 2003). No sapropelitic and tephra layers occur at Hole 963D and in material used for the present study (the upper 3.55 m of the sedimentary sequence), although they are present in older levels recovered at Site 963A (Emeis et al., 1996; Tamburrino et al., 2012).

Planktonic (*Globigerinoides ruber* sensu stricto and *Neogloboquadrina incompta*) and benthic (*Uvigerina mediterranea*) foraminifera have been analyzed for their oxygen and carbon isotope compositions. Analyses for Core 963D were performed by a PDZ Europa Geo2020 mass spectrometer at the Southampton Oceanography Centre, with an individual acid bath carbonate preparation. The selected specimens were cleaned using an ultrasonic bath, and thoroughly dried batches of 7–10 specimens (picked up from the fraction between 150 and 300 μm) were loaded into quartz vials for reaction with orthophoshoric acid at 70°C. Calibration to the Vienna Pee Dee Belemnite (VPDB) was carried out by NBS-19 standards. For both $\delta^{13}C$ and $\delta^{18}O$ external precision is better than 0.06‰.

Ice volume-corrected (ivc) oxygen isotope data of different species were calculated by the conversion of $\delta^{18}O$ to relative sea level in the eastern Mediterranean (Rohling et al., 2014). Specifically, the equations $y = -54.33006067x + 2.144129497x^2$ and $y = -61.74158411x + 3.12127659x^2$ were, respectively, calculated for *G. ruber* and *N. incompta*, where x is the oxygen isotope value and y is the relative sea level. A constant 0.009‰ correction per meter of sea level change was applied to *U. mediterranea* $\delta^{18}O$ values (Rohling et al., 2014). Sea level variations were selected from Lambeck et al. (2014).

3. Local Setting

The negative hydrological balance is the main feature that controls the Mediterranean antiestuarine circulation pattern (Robinson & Golnaraghi, 1994). MAW enters the Gibraltar Strait and occupies the upper 200 m of the water column (Figure 1a). In the Alboran Sea, MAW flows along the North African coast and reaches the Sicily Strait (Millot, 1999). Into the Sicily Channel, the northern branch of MAW (Atlantic Ionian Stream) flows toward the Ionian Sea and later toward the Levantine basin (Malanotte-Rizzoli et al., 2014;

Table 1
The ^{14}C AMS Radiocarbon Ages and Their Calibrated Values After the Bayesian Deposition Model by OxCal 4.3.2 (Reimer et al., 2013)

Reference	Site	Core	Section/interval	C14 age (BP)	Calibrated age (BP)[a] 1-sigma
Incarbona et al. (2008)	ODP 963D	1H	S1 2-4	1,500 ± 40	1,055 ± 60
Incarbona et al. (2008)	ODP 963D	1H	S1 55-56	2,810 ± 90	2,549 ± 105
Incarbona et al. (2008)	ODP 963D	1H	S1 106-107	4,320 ± 65	4,455 ± 85
Incarbona et al. (2008)	ODP 963D	1H	S1 142-143	5,380 ± 75	5,748 ± 85
Incarbona et al. (2008)	ODP 963D	1H	S2 48-50	7,510 ± 50	7,956 ± 50
Incarbona et al. (2008)	ODP 963D	1H	S3 23-24	10,080 ± 100	11,059 ± 110

[a]Bayesian deposition model by OxCal 4.3.2 (Ramsey, 2008), Marine 13 (Reimer et al., 2013), DR = 0 (G. Siani, 2019, personal communication, June 2019).

Pinardi & Masetti, 2000). LIW formation occurs in the eastern basin (Figure 1b), usually in February–March due to surface cooling of salt-enriched water masses (Malanotte-Rizzoli et al., 2014; Malanotte-Rizzoli & Hecht, 1988), and is established at 200–600 m depth. LIW crosses the Sicily Channel together with a thin layer of Eastern Mediterranean Deep Water (EMDW) and flows into the Tyrrhenian Sea (Gasparini et al., 2005; Lermusiaux & Robinson, 2001; Millot, 1999). LIW maintains almost unaltered values of temperature and salinity (13.2–13.5°C and about 38.5‰) from the Ligurian Sea and the Gulf of Lions to the Balearic and Alboran Seas (Millot, 1999) and is the main source of Mediterranean Outflow Water, which passes through the Gibraltar Strait. Deep water formation takes place in the Gulf of Lions (WMDW) and in the Adriatic and Aegean Seas (EMDW), where permanent cyclonic gyres are established (Figure 1b). In these regions, Mistral, Bora, and Etesian winds produce water column convection. Surface water mixes up with LIW and sinks to the seafloor (Malanotte-Rizzoli et al., 2014; Pinardi & Masetti, 2000; Rohling et al., 2015).

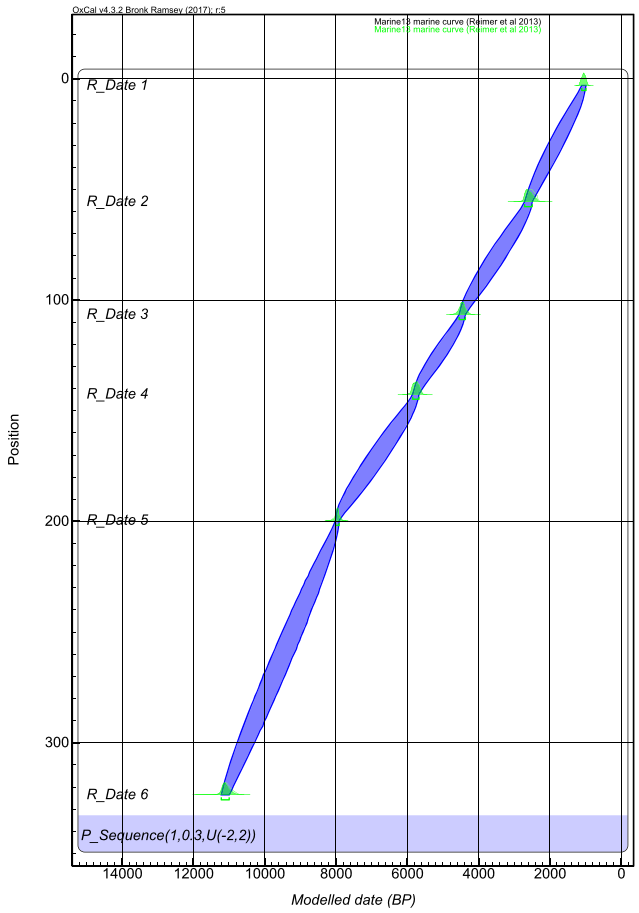

Figure 2. Depth/age plot of the Bayesian deposition model assessed by OxCal 4.3.2 (Ramsey, 2008). "Position" on the *y* axis refers to cmbsf. See Table 1 for the ^{14}C AMS radiocarbon ages adopted in the model. Each modeled calibrated age is reported with their highest probability density range (green curve) and the 1-σ uncertainty (green line). The blue-violet shadow shows the error propagation at 1σ.

4. Chronology

The chronological framework is based on six dated horizons. Radiometric ages and their uncertainties were probabilistically assessed in a Bayesian deposition model by OxCal4.3.2 (Ramsey, 2008). The Marine 13 calibration curve (Reimer et al., 2013), with $\Delta R = 0$ (Giuseppe Siani, 2019; Siani et al., 2000, personal communication) was applied. The "Agreement Index" that establishes the statistical robustness of the model between unmodeled and modeled data (Ramsey, 2008) is >99%. The age mismatch for all tie points, with respect to the earlier calibration by Incarbona et al. (2008), is always <20 years (Table 1). The error propagation at 1σ is < ±320 years from the base of the record up to 5.75 ka, < ±230 between 5.75 and 4.5 ka and between 2.5 and 1.0 ka, and < ±290 between 4.5 and 2.5 ka (Figure 2). Sedimentation rates range between 25.8 and 40.0 cm/kyr corresponding to resolution of, respectively, 39 and 25 years per 1 cm. The average sampling resolution is of 84 years for *G. ruber* and *U. mediterranea* measurements and of 115 years for *N. incompta*.

Benthic foraminifera from the Aegean Sea LC21 core (Figure 1b) (Abu-Zied et al., 2008) are plotted following the age model by Grant et al. (2012). Differently from the present paper, Grant et al. (2012) used the Marine09 calibration curve. However, Marines 13 and 09 curves are nearly identical one each other over the last 12 kyr. Total di- and tri-alkenones and alkenone-derived sea surface temperature

(SST) from the Alboran Sea ODP Site 976 and MD95-2043 cores (Figure 1b) (Cacho et al., 1999, 2002, Martrat et al., 2004, 2014) are plotted following the chronology by Martrat et al. (2014). All the other records used in the figures for comparison follow their original chronology.

5. Ecology of Species Used for the Geochemical Analysis

The $\delta^{18}O$ of foraminifera shells reflects the oxygen isotopic composition of the seawater and the temperature in which they calcify. The $\delta^{13}C$ of foraminifera shells reflects the carbon isotopic composition of the dissolved inorganic carbon (DIC) in which they calcify. Thus, the habitat of species used for the analysis is a basic requirement for the correct interpretation of the geochemical signal. In the following, we report a short summary of the ecological preferences of *G. ruber*, *N. incompta* and *U. mediterranea*.

G. ruber thrives in warm and oligotrophic waters (Hemleben et al., 1989; Žarić et al., 2005). In the Mediterranean Sea, *G. ruber* is abundant or dominant in surface water above the summer thermocline (Pujol & Grazzini, 1995; Rigual-Hernández et al., 2012). *N. incompta* proliferates in a distinct deep chlorophyll maximum layer (Fairbanks & Wiebe, 1980; Rohling & Gieskes, 1989) and in winter/spring is abundant in the western Mediterranean Sea (Pujol & Grazzini, 1995; Rigual-Hernández et al., 2012). Water samples collected in the Sicily Strait during the VICOMED I and II expeditions show that *N. incompta* accounts for a total of 4.6% of the total planktonic foraminifera assemblage in winter/spring and that its occurrence is negligible in summer/fall (Pujol & Grazzini, 1995).

U. mediterranea is a shallow infaunal benthic species, mostly confined to the topmost 1 cm of sediment, that prefers mesotrophic environments (De Rijk et al., 2000; Fontanier et al., 2008; Jorissen, 1999; Kuhnt et al., 2007; Schmiedl et al., 2000, 2004). In the Mediterranean Sea, this species occurs at a shallower depth from the western to the eastern basin, following the organic matter flux decrease (De Rijk et al., 2000). The *U. mediterranea* $\delta^{13}C$ record, like other shallow infaunal species, reflects a process of organic matter remineralization in pore waters (Fontanier et al., 2006; Pérez-Asensio et al., 2020; Schmiedl et al., 2004; Theodor, Schmiedl, Jorissen, et al., 2016, Theodor, Schmiedl, & Mackensen, 2016). The DIC $\delta^{13}C$ in pore water is controlled by bottom water $\delta^{13}C_{DIC}$ and by the decomposition of ^{12}C-enriched organic matter, revealing a gradient of about 1‰ per 1 cm in the upper part of surface sediments (Fontanier et al., 2006; Schmiedl et al., 2004). Benthic foraminifera shallow infaunal $\delta^{13}C$ values are used as a qualitative productivity proxy in paleoproductivity reconstructions, especially when they take into account the difference with $\delta^{13}C$ values of epifaunal species (Le Houedec et al., 2020; Pérez-Asensio et al., 2020; Theodor, Schmiedl, Jorissen, et al., 2016, Theodor, Schmiedl, & Mackensen, 2016). However, bottom water oxygen content is a further parameter that affects $\delta^{13}C$ in pore water, and its variability significantly produces a bias in paleoproductivity reconstructions (McCorkle & Emerson, 1988; Schmiedl et al., 2004).

6. Results and Discussion

6.1. The Isotopic Record

The oxygen isotopic records acquired on foraminifera shells of the surface dweller *G. ruber*, the deep chlorophyll maximum grazer *N. incompta* and the benthic *U. mediterranea* from the ODP Site 963, are presented in Figure 3. The $\delta^{18}O$ records reflect different species habitats in the water column. The highest variability of *G. ruber* reflects the presence of fresh and warm lenses in the topmost water column (Emeis et al., 2003; Rodríguez-Sanz et al., 2017; Rohling et al., 2004). The stability in the *U. mediterranea* signal is likely due to decadal-scale homogenization of winter water established at intermediate depth that smooths short-term variability in temperature and salinity and produces a stable and averaged record (Rohling et al., 2004). This is not the case for the $\delta^{18}O$ record of *N. incompta*, often associated to intermediate water, where a short-term variability is evident. The correlation index between *N. incompta* and *U. mediterranea* $\delta^{18}O$ ($R^2 = 0.80$, $n = 73$; Figure 4a) reveals the close relationship of the two species that inhabit the same water mass, but the *N. incompta* habitat should be located at the top of intermediate water where a continuous mixing with surface water is likely (the correlation index between *N. incompta* and *G. ruber* $\delta^{18}O_{ivc}$ is $R^2 = 0.62$, $n = 71$; Figure 4b). The difference in the oxygen isotopic composition between *U. mediterranea* and *G. ruber* $\delta^{18}O$ is quite evident (Figure 3). A weak positive correlation index still exists between the two species ($R^2 = 0.32$, $n = 101$; Figure 4c), likely due to occasional homogenization of the whole Sicily

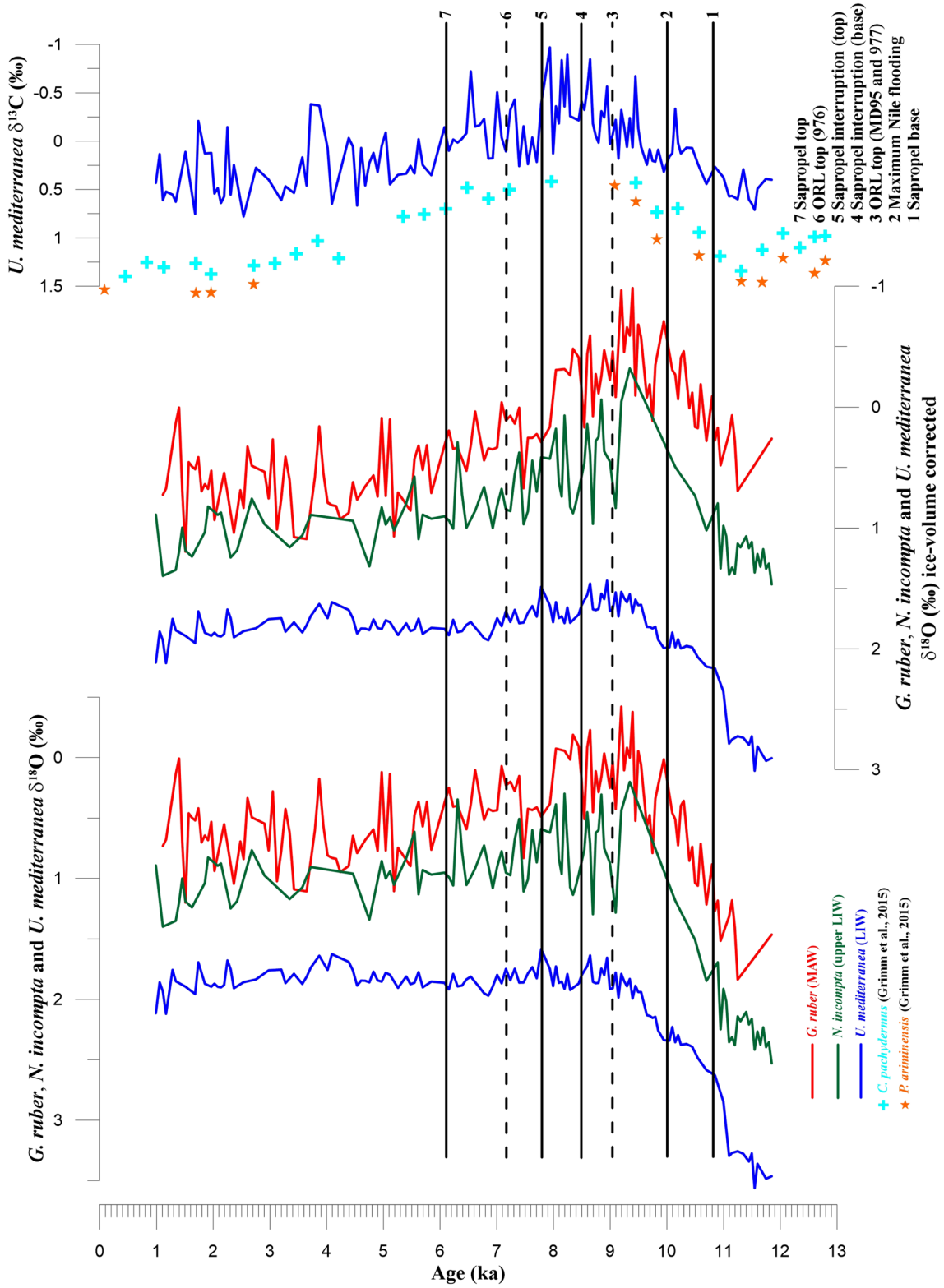

Figure 3. Downcore variations of planktonic and benthic $\delta^{18}O$ raw data, $\delta^{18}O_{IVC}$, and $\delta^{13}C$ at ODP Hole 963D plotted versus age (ka). Blue lines show *U. mediterranea* $\delta^{18}O$ raw data, $\delta^{18}O_{IVC}$, and $\delta^{13}C$ values (this study). Green lines are *N. incompta* $\delta^{18}O$ raw data and $\delta^{18}O_{IVC}$ values (this study). Red lines are *G. ruber* $\delta^{18}O$ raw data and $\delta^{18}O_{IVC}$ values (this study). Cyan plus signs and orange stars, respectively, refer to *C. pachydermus* and *P. ariminensis* $\delta^{13}C$ values from Grimm et al. (2015). Black solid, dashed, and dotted lines refers to selected events in the western and eastern Mediterranean Sea during sapropel and ORL deposition, as discussed in the text.

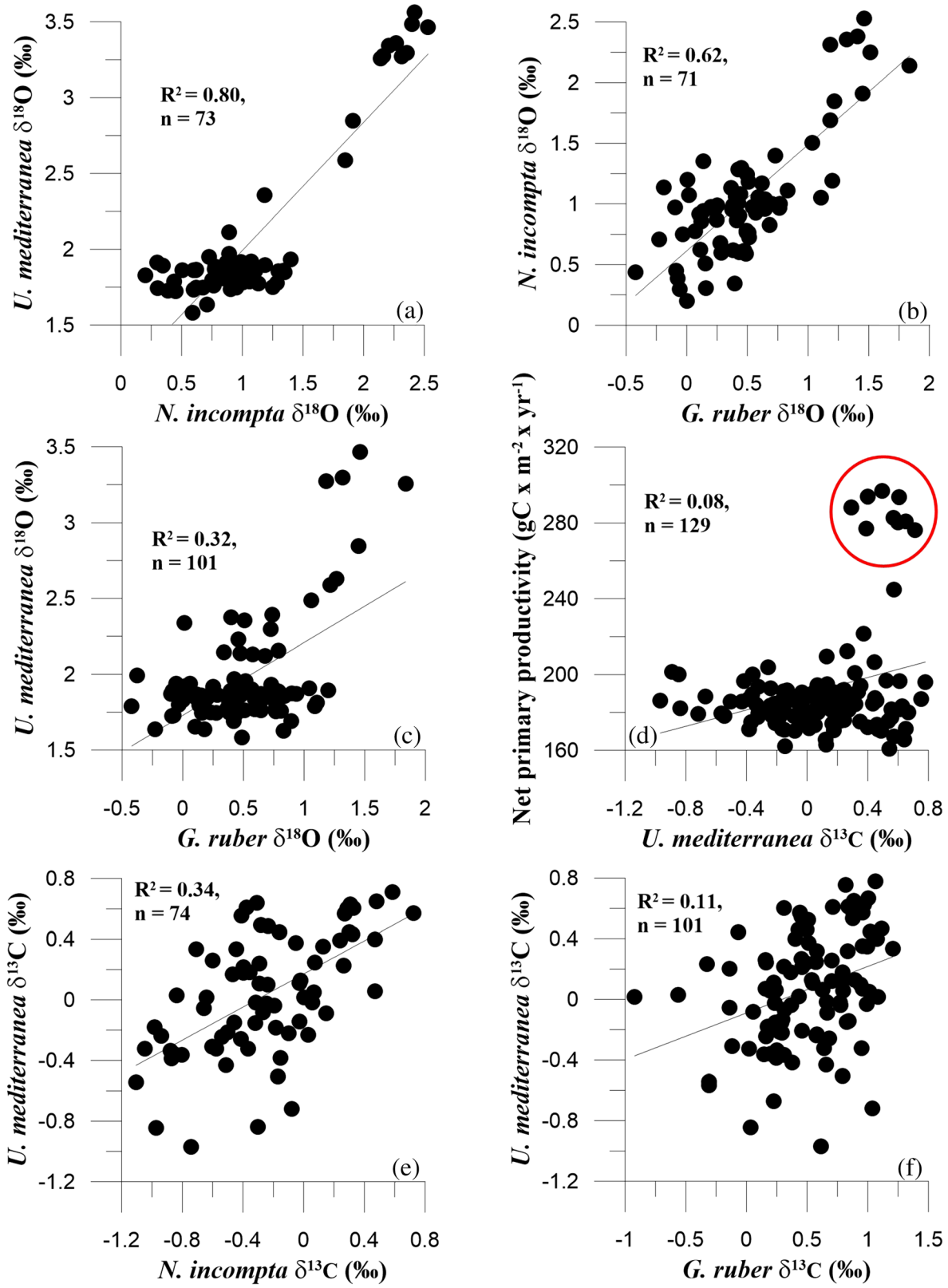

Figure 4. Scatter plots of $\delta^{18}O$ values for different foraminifera species (a–c), of *U. mediterranea* $\delta^{13}C$ values and net primary productivity (Incarbona et al., 2008) (d) at Hole 963D and of $\delta^{13}C$ values for different foraminifera species (e, f). The correlation index is also shown. The red circle in (d) shows the highest productivity recorded during the Younger Dryas, associated with positive *U. mediterranea* $\delta^{13}C$ values.

Channel water column and to response to the same regional/global climatic trends. The latter phenomenon is for instance recorded during the early Holocene, when regional warming and freshening (Emeis et al., 2000; Marino et al., 2009; Martrat et al., 2004) led to a significant depletion (>1‰) in isotopic signals of both MAW and LIW (Figure 3).

The $\delta^{18}O_{IVC}$ depends on both the local/regional seawater $\delta^{18}O$ and the temperature of the water mass in which the foraminifera shell calcifies. The seawater $\delta^{18}O$ is the result of different processes, such as the precipitation/evaporation ratio, river runoff, and the isotopic composition of Atlantic water inflow. In the today's Mediterranean Sea, the correlation index between seawater $\delta^{18}O$ and salinity is $R^2 = 0.695$, $n = 131$ (LeGrande & Schmidt, 2006). It is likely that this relationship has changed in the past (Emeis et al., 2000; Rohling & Bigg, 1998) and this is certainly true during sapropel deposition, when a large amount of freshwater was discharged into the basin. The estimate for the freshwater discharge of sapropel S5 accounts for about nine times the modern pre-Aswan Nile discharge (Amies et al., 2019). In this scenario, low salinity was definitively the leading factor for depleted foraminifera and seawater $\delta^{18}O$ values, while only the temperature concentration effect, which is limited to the top water column, may have affected the *G. ruber* $\delta^{18}O$ (Amies et al., 2019). Though a smaller amount of freshwater was discharged for sapropel S1 (Rohling et al., 2015), the same salinity prevalence would be expected. Since our discussion is mainly addressed to the identification of intermediate water changes in the *U. mediterranea* and *N. incompta* $\delta^{18}O_{IVC}$, the temperature concentration effect is largely negligible.

It is not possible to decompose the single contribution of temperature and salinity to the $\delta^{18}O_{IVC}$ of the three foraminifera species in the Sicily Channel. However, we note that temperature and salinity changes would have operated in a coherent manner to drive calcite and seawater $\delta^{18}O$ modification over the early-middle Holocene. In fact, it is well-established that during the early Holocene insolation peak, while the Nile River was flooding the eastern Mediterranean Sea (Weldeab et al., 2014) and there was an increased river discharge in the Mediterranean northern borderlands (Filippidi & De Lange, 2019; Magny et al., 2011; Toucanne et al., 2015; Wagner et al., 2019), SST increased in both the western and eastern basins (Marino et al., 2009; Martrat et al., 2004, 2014). Increased SST and reduced salinity for river runoff would have acted together for calcite and seawater $\delta^{18}O$ depletion. In exactly the opposite way, cooling and monsoon weakening episodes, like during the 8.2 ka event, would have mutually operated to increase calcite and seawater $\delta^{18}O$ values. Decoupling of SST between the eastern and western Mediterranean has been observed during Termination II (TII) (Rodríguez-Sanz et al., 2017). This may cast suspicion on a possible similar behavior during TI, but the time interval eventually involved for such a phenomenon, between ~18.0 and 14.5 ka (Stern & Lisiecki, 2014), is distinctly earlier than the time interval here investigated and discussed (about 10.0–6.5 ka). The same time interval offset with the early-middle Holocene deals with the isotopically light meltwater inflow from the Atlantic Ocean that occurred during the HE1 deposition, between ~17.0 and 15.0 ka (Hodell et al., 2017), and crossed the western-central Mediterranean (Sierro et al., 2005; Sprovieri et al., 2012).

The single contribution of SST and salinity to the seawater and calcite $\delta^{18}O$ cannot be quantitatively addressed because of multiple possible caveats above described. However, we are confident that the $\delta^{18}O_{IVC}$ records still represent a qualitative estimate of water mass density and in fact they reflect the vertical location of the three species along the water column (Figure 3). The $\delta^{18}O_{IVC}$ profiles still maintain trends and high-frequency variability of the original oxygen isotopic data.

The *U. mediterranea* $\delta^{13}C$ record ranges between −0.97‰ and 0.78‰, 0.09‰ on average, and shows a distinct high-frequency variability (Figure 3). The *U. mediterranea* $\delta^{13}C$ gets more depleted to ~8.0 ka, and the subsequent enrichment is similar to the trend observed in less-resolved epifaunal species *Planulina ariminensis* and *Cibicidoides pachydermus* in the Sicily Channel SL78 core (Grimm et al., 2015). As commented above, in section 5, the *U. mediterranea* $\delta^{13}C$ may be a qualitative productivity proxy under constant seafloor oxygen content. Holocene productivity at Site 963 has been estimated by a coccolith-based transfer function (Incarbona et al., 2008). The comparison between *U. mediterranea* $\delta^{13}C$ and the net primary productivity estimates does not show any evident relationship (Figure 5), and the correlation coefficient is $R^2 = 0.08$, $n = 129$ (Figure 4d). This result may rely upon the very small magnitude of productivity changes observed in the Sicily Channel throughout the Holocene (<40 gC x m^{-2} x $yearr^{-1}$), but it is also in line with previous reports of a limited effect of local productivity on the *Uvigerina* spp. $\delta^{13}C$ variability in strongly advective

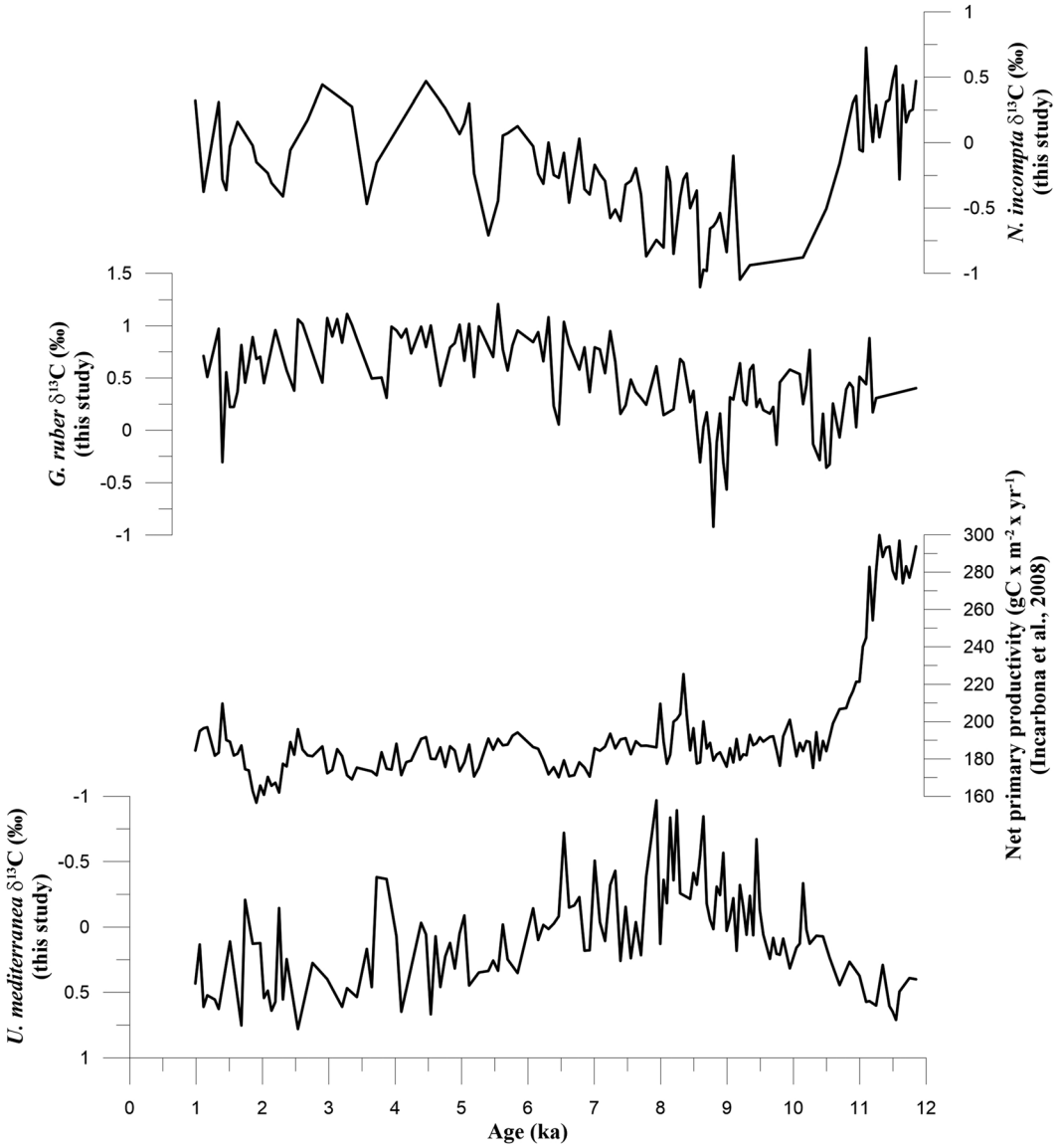

Figure 5. Downcore variations of *U. mediterranea*, *G. ruber*, and *N. incompta* $\delta^{13}C$ values (this study) and net primary productivity values (Incarbona et al., 2008) at ODP Hole 963D plotted versus age (ka).

environments (Hall et al., 2001; Mackensen et al., 1993; Toucanne et al., 2012). Both the highest net primary productivity pulse at ODP Site 963 recorded during the latest Younger Dryas and the subsequent decrease, which exceeded 100 gC x m^{-2} x $year^{-1}$, across the Younger Dryas/Holocene transition, show a relationship with *U. mediterranea* $\delta^{13}C$ data that is opposite to what should be expected by a productivity control: Carbon isotopic ratio was at maximum values during the Younger Dryas and decreased rapidly during the early Holocene (see red circle in Figure 4d and Figure 5). Any evident relationship is also missing or opposite with planktonic species $\delta^{13}C$ (Figures 4e, 4f, and 5), whose high values would indicate enhanced productivity in sea surface (*G. ruber*) and in the DCM layer (*N. incompta*), since a high photosynthesis rate depletes ^{12}C in the photic zone.

Thus, we are confident that the *U. mediterranea* $\delta^{13}C$ at ODP Hole 963D is significantly affected by bottom water (LIW) ventilation and gives insight into Mediterranean zonal circulation rates at depth. This assumption is further supported by the adoption of *Uvigerina* spp. $\delta^{13}C$ as a proxy of bottom water ventilation over the last 130 kyr in the Corsica Trough, a location whose seafloor is equally crossed by LIW (Toucanne et al., 2012).

6.2. Isotopic Record of Intermediate Water During Sapropel S1 Deposition and ORL Termination

The antiestuarine Mediterranean circulation pattern has never been reversed during late Quaternary sapropels, as visible in modeling and outflow water in the Gulf of Cadiz (Myers et al., 1998; Schönfeld & Zahn, 2000; Zahn et al., 1987). Thus, the *G. ruber* $\delta^{18}O_{ivc}$ depletion since the early Holocene (Figure 6a), indicative of MAW lower density, should be imputable to global/regional warming and freshening. SSTs from the Alboran Sea show the highest values since 9.3 ka (Martrat et al., 2004) (Figure 6b), but even enhanced precipitation and/or local river runoff may have contributed to *G. ruber* $\delta^{18}O_{ivc}$ depletion (Di Donato et al., 2019; Filippidi & De Lange, 2019; Maiorano et al., 2019; Sha et al., 2019; Toucanne et al., 2015; Wagner et al., 2019). The great visual similarity between the Sicily Channel *G. ruber* $\delta^{18}O_{ivc}$ and the Alboran Sea SST records (Figures 6a and 6b) would point to a major control by the thermal character of inflowing Atlantic surface water. However, following the Bemis et al. (1998) calculation (0.2‰ × 1°C), the wide excursion of *G. ruber* $\delta^{18}O$ values would largely exceeds the ~2.5°C warming of the Alboran Sea alkenone-derived SSTs (Figures 6a and 6b). The discrepancy may be, at least partially, reconciled considering that (1) the alkenone SST increase in the Sicily Channel from the late Younger Dryas to the early Holocene seems to be greater than the Alboran Sea (Sicre et al., 2013); (2) a more pronounced warming in summer, following the *G. ruber* ecological preference (Hernández-Almeida et al., 2011; Pujol & Grazzini, 1995), with respect to winter/spring alkenone-derived temperatures (Incarbona, Jonkers, et al., 2019; Knappertsbusch, 1993; Ziveri et al., 2000); and (3) the wide excursion of *G. ruber* $\delta^{18}O$ values may reflect a temperature concentration effect in the upper summer mixed layer, like for sapropel S5 (Amies et al., 2019; Rodríguez-Sanz et al., 2017).

The *N. incompta* and *U. mediterranea* $\delta^{18}O_{ivc}$ and the *U. mediterranea* $\delta^{13}C$ records (Figure 3), indicative of LIW density and Sicily Channel seafloor ventilation, seem to be mostly controlled by sapropel S1 dynamics. Significant decreases of these records are visible since the sapropel S1 onset at 10.8 ka (De Lange et al., 2008; Rohling et al., 2015) and since the maximum Nile River flooding at 10.0 ka (Weldeab et al., 2014). These stable isotopic decreases in the LIW testifies to the production of a less dense (shallower) water mass and a slower zonal vertical circulation belt (decreased water exchange across the Sicily Strait) during sapropel S1 deposition, in line with the conclusions from neodymium isotopes from eastern and western Mediterranean sites and from paleocirculation modeling (Dubois-Dauphin et al., 2017; Myers et al., 1998; Vadsaria et al., 2019; Wu et al., 2019).

The sapropel deposition was interrupted from 8.5 to 7.8 ka, due to restored deep water formation in the Adriatic and/or Aegean Seas and reestablished oxygenation above 1,500–1,800 m depth, after monsoon activity weakening and/or northern outbreak occurrence (Casford et al., 2003; De Lange et al., 2008; Filippidi et al., 2016; Filippidi & De Lange, 2019; Le Houedec et al., 2020; Rohling, Mayewski, et al., 2002, 2015). In the Sicily Channel, *N. incompta* and *U. mediterranea* $\delta^{18}O_{ivc}$ data suggest the occurrence of a denser LIW, as well as the *U. mediterranea* $\delta^{13}C$ record that testifies to risen LIW circulation (Figure 3). The 8.2 ka event is even visible in the *G. ruber* $\delta^{18}O_{ivc}$ record, though with a different, and possibly contrasting, manner (Figure 3). However, the *G. ruber* $\delta^{18}O_{ivc}$ signal is almost identical to the Alboran Sea SSTs (Figures 6a and 6b), once again suggesting the its different (MAW) origin with respect to the LIW origin of the *N. incompta* and *U. mediterranea* $\delta^{18}O_{ivc}$ signal.

Sapropel S1 deposition ended at ~6.1 ka, with the oxygen restoration on the eastern Mediterranean seafloor below 1,500–1,800 m depth (De Lange et al., 2008; Rohling et al., 2015). This horizon may also be distinguished in the ODP 963 record and coincides with heavier *N. incompta* $\delta^{18}O_{ivc}$ values or with positive values in the *U. mediterranea* $\delta^{13}C$ curve (Figure 3). However, the most prominent shift in the *U. mediterranea* $\delta^{13}C$ profile occurs earlier, at about 6.5 ka (Figure 3), an age that is compatible with the full reoxygenation of bottom waters at intermediate depths, above ~800 m (Filippidi & De Lange, 2019).

The most recent ORL onset started in coincidence with the meltwater pulse 1a and the Bølling-Allerød beginning, at ~14.5 ka (Cacho et al., 2002; Jimenez-Espejo et al., 2008; Martrat et al., 2014). The ORL layer is preferentially identified by the increased alkenone accumulation in the western Mediterranean Sea; that in the Alboran Sea is arranged in two maxima separated by a late Younger Dryas-early Holocene "saddle" (Figures 6c and 6d). The alkenone accumulation in the Alboran Sea abruptly finished at ~9.0 ka in ODP Site 977 (black line in Figure 6c) and MD95-2043 (Cacho et al., 2002; Martrat et al., 2014). At the ODP Site 976 the ORL is prolonged, with a first alkenone decrease coinciding with the sapropel S1 interruption

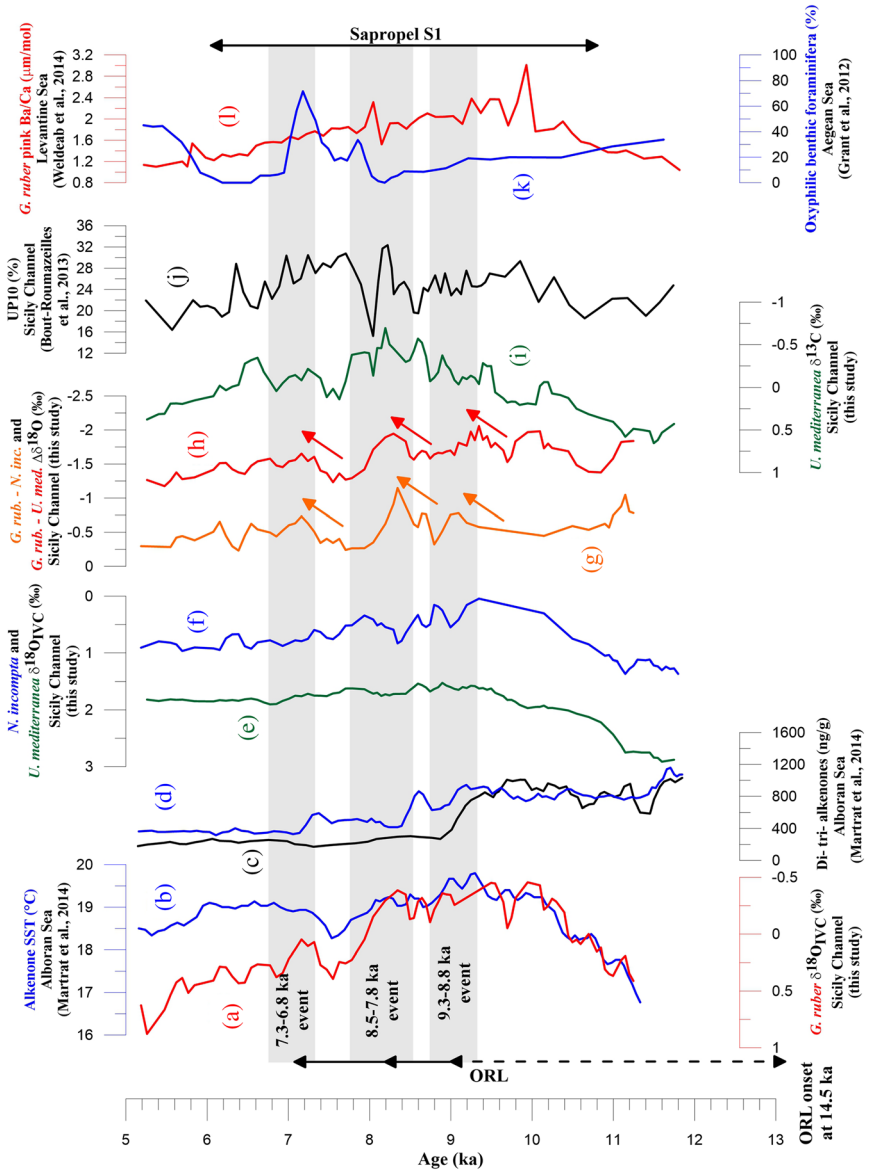

Figure 6. Downcore variations of planktonic and benthic $\delta^{18}O_{IVC}$ and $\delta^{13}C$ at ODP Hole 963D plotted versus age (ka) and comparison with eastern and western Mediterranean selected geochemical, sedimentological, and micropaleontological records. (a) Three-point running average (red line) of *G. ruber* $\delta^{18}O_{IVC}$ (this study). (b) Three-point running average of alkenone-derived SSTs in the AlboranSea record ODP 976 (blue line) (Martrat et al., 2014). (c) Three-point running average of total di- and tri-alkenones at the MD95-2043 site (black line) (Cacho et al., 2002; Martrat et al., 2014). (d) Three-point running average of total di- and tri-alkenones at the ODP 976 site (blue line) (Cacho et al., 2002; Martrat et al., 2014). (e) Three-point running average (green line) of *U. mediterranea* $\delta^{18}O_{IVC}$ (this study). (f) Three-point running average (blue line) of *N. incompta* $\delta^{18}O_{IVC}$ (this study). (g) Difference between *G. ruber* $\delta^{18}O$ and *N. incompta* $\delta^{18}O$ (orange line) (this study). Orange arrows show the increased stratification at the beginning of the three 9.3–8.8, 8.5–7.8, and 7.3–6.8 ka intervals. (h) Difference between *G. ruber* $\delta^{18}O$ and *U. mediterranea* $\delta^{18}O$ (red line) (this study). Red arrows show the increased stratification at the beginning of the three 9.3–8.8, 8.5–7.8, and 7.3–6.8 ka intervals. (i) Three-point running average (green line) of *U. mediterranea* $\delta^{13}C$ (this study). (j) UP10 sortable silt fraction in the Sicily Channel MD04-2797CQ core (Bout-Roumazeilles et al., 2013). (k) Three-point running average (blue line) of oxyphilic benthic foraminifera from the Aegean core LC21 (Abu-Zied et al., 2008; Casford et al., 2003), plotted following the chronology by Grant et al. (2012). (l) *G. ruber* pink Ba/Ca (red line) in core SL 112, Levantine Sea (Weldeab et al., 2014). Light gray vertical bands indicate the three 9.3–8.8, 8.5–7.8, and 7.3–6.8 ka perturbation intervals discussed in the text. Black arrows in western and eastern Mediterranean records indicate the chronological extent of sapropel S1 and ORL deposition. The dashed black arrow in the ORL box indicates that the onset at 14.5 ka is not illustrated in the plot. The three black arrows in the upper part of the ORL box show possible terminations discussed in the text.

(~8.2 ka) and a final drop at ~7.2 ka (Martrat et al., 2014) (blue line in Figure 6d). In other sites from the Alboran and Balearic Seas, the ORL termination is reported at ~8.2 ka on the basis of TOC profiles, with minor organic carbon accumulation that continued up to ~7.6–7.3 ka (Jimenez-Espejo et al., 2007, 2008). This apparently puzzling framework for the end of the ORL is likely due to local productivity pulses with enhanced oxygen demand for organic matter remineralization and decoupling of ventilation at intermediate and deep water layers (Pérez-Asensio et al., 2020). In any case, the demise of the ORL is confidently ascribed to bottom water reventilation that occurred in both intermediate and deep western Mediterranean sites between 9.2 and 7.6 ka (Pérez-Asensio et al., 2020).

The ORL termination at Site 977 and MD95-2043 core matches with a double peak in LIW denser water and improved zonal circulation in the Sicily Channel, between 9.3 and 8.8 ka (Figures 6e, 6f, and 6i). In the Levantine Basin, the base of this interval marks the end of the Nile River maximum flooding (Figure 6l) (Weldeab et al., 2014). The 8.2 ka event, coinciding with the 8.5–7.8 ka sapropel interruption and seafloor reventilation at intermediate depths (Abu-Zied et al., 2008; Casford et al., 2003; Filippidi & De Lange, 2019; Incarbona, Abu-Zied, et al., 2019; Le Houedec et al., 2020; Rohling et al., 2015; Zirks et al., 2019), is characterized by increasing LIW density and improved bottom ventilation in the Sicily Channel (Figures 6e, 6f, and 6i). The final alkenone accumulation in the ODP Site 976 occurred between7.3 and 6.8 ka and matches with a prominent peak in the Aegean Sea oxyphilic benthic foraminifera (Figure 6k) (Abu-Zied et al., 2008; Casford et al., 2003), with geochemical and micropaleontological evidence of deep water formation in the Adriatic Sea (Di Donato et al., 2019; Filippidi & De Lange, 2019; Maiorano et al., 2019) and again with increasing LIW density and improved seafloor ventilation in the Sicily Channel (Figures 6e, 6f, and 6i). The 8.2 and 7.2 ka events, which led to benthic foraminifera repopulation, are compatible with improved deep water oxygenation in the Adriatic and Aegean Sea (Filippidi et al., 2016; Filippidi & De Lange, 2019). Changes in the Sicily Channel seafloor and in the eastern Mediterranean hydrological and micropaleontological records suggest the occurrence of regional (pan-Mediterranean) perturbations, rather than local western Mediterranean phenomena, for explaining the ORL termination.

Increased stratification between MAW and LIW marks the beginning of all three 9.2, 8.2, and 7.2 ka events, as visible in the higher oxygen isotopic difference between *G. ruber* and *U. mediterranea* ($\Delta\delta^{18}O_{G.rub\text{-}U.med}$) and between *G. ruber* and *N. incompta* ($\Delta\delta^{18}O_{G.rub\text{-}N.inc}$) (see red and orange arrows in Figures 6g and 6h). It would be expected that thermohaline circulation slowdown matches with increased water column stratification, and vice versa, like for the eastern Mediterranean Sea during the deposition of sapropel S1 (Grimm et al., 2015; Le Houedec et al., 2020; Rohling et al., 2015; Rohling & Gieskes, 1989). However, the Sicily Channel behavior is opposite due to its peculiar hydrological setting: There is not any deep water convection cell, like in the western and eastern basins, and a two layer circulation (at surface and intermediate depth) is forced across the Strait with an opposite path of the water masses. As observed for last glacial stadials and Heinrich events, and as observed for EMT-like events over the last five centuries, the strengthened Mediterranean thermohaline circulation leads to the advection of fresher (less modified/evaporated) MAW and saltier LIW, increasing their density contrast and water column stratification (Incarbona et al., 2013, 2016).

In Figure 7 we focus on the 10.0–6.5 ka time interval. The three intervals above described (9.3–8.8, 8.5–7.8, and 7.3–6.8 ka) show distinctive episodes of activity weakening in the West Africa and Indian monsoons (Figures 7b and 7f) (Fleitmann et al., 2003; Weldeab et al., 2007). We argue that after the transit through the Sicily Channel, denser LIW and strengthened zonal circulation (Figure 7c) may have promoted deep water formation in the Gulf of Lions. The Balearic Sea UP10 sortable silt indicates the recovery of sea bottom circulation in the western Mediterranean meridional cell since the 9.2 ka event, after a long period of slowdown (Frigola et al., 2008). The intensification of western Mediterranean seafloor circulation is prolonged up to ~8.0 ka, without distinction of the 9.2 and 8.2 ka events (Figure 7a). However, this apparent continuation is due to relatively low-resolution and lacking samples analyzed between 8.7 and 8.5 ka, in the interval that marks the passage between the two events (see symbols in Figure 7a). The higher resolution of the Sicily Channel UP10 record, where a distinct peak for enhanced bottom circulation at ~8.6 ka exists (Figure 6j), supports the possible shortcoming of the Balearic Sea sortable silt record in this interval.

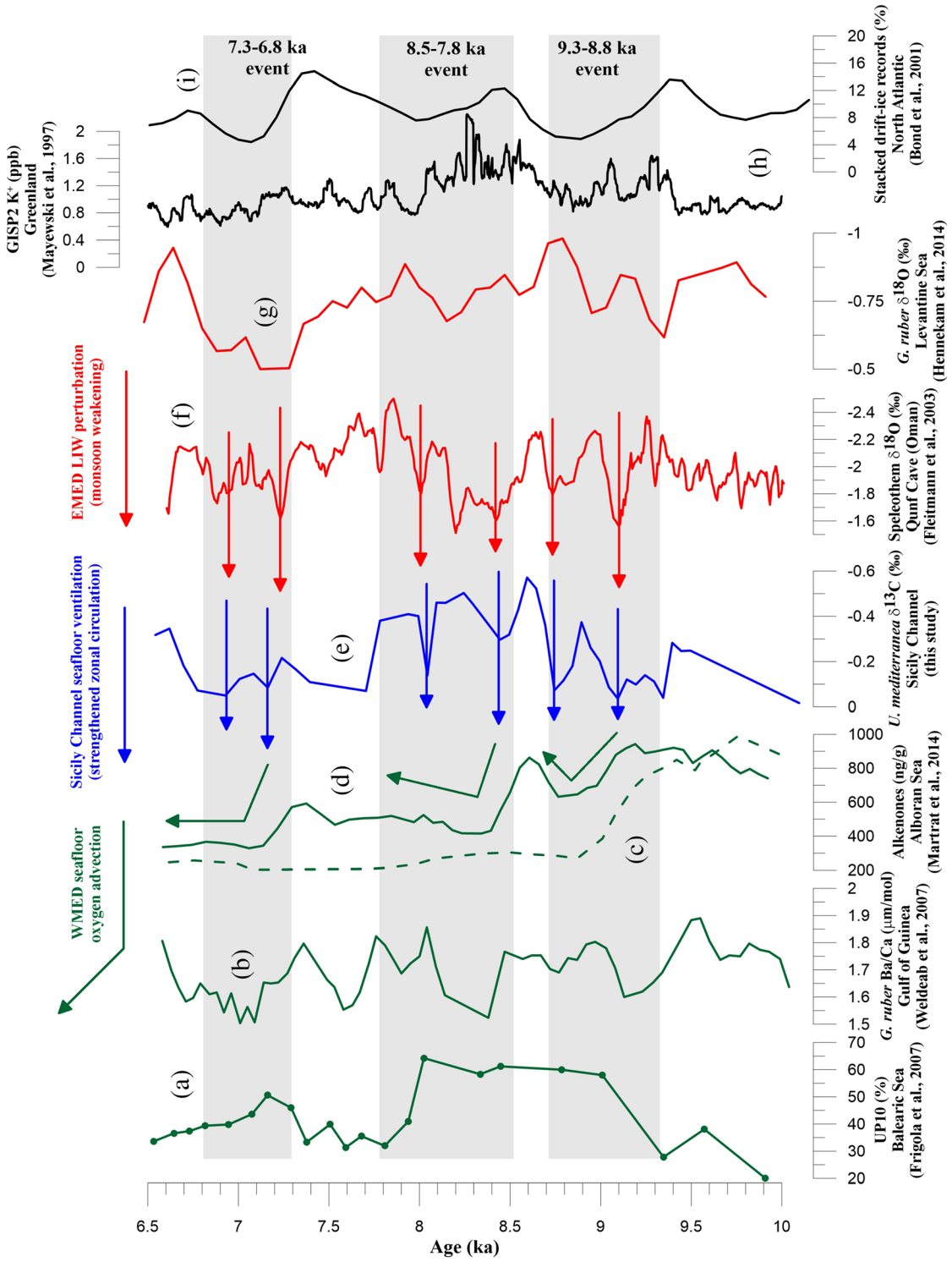

Figure 7. Downcore variations of benthic $\delta^{13}C$ at ODP Hole 963D zoomed on the 10.0–6.5 ka interval and its comparison with selected Mediterranean and extra-Mediterranean geochemical and sedimentological records. (a) UP10 sortable silt fraction (green line) in the Balearic Sea MD99-2343 core (Frigola et al., 2008). Dots indicate analyzed samples. (b) *G. ruber* Ba/Ca (green line) in the Gulf of Guinea (Weldeab et al., 2007). (c and d) Three-point running average of total di- and tri-alkenones at ODP 976 (green solid line) and MD95-2043 (green dashed line) (Cacho et al., 2002; Martrat et al., 2014). (e) Three-point running average of *U. mediterranea* $\delta^{13}C$ (blue line) (this study). (f) Five-point running average of $\delta^{18}O$ in Qunf Cave (Oman) speleothems (red line) (Fleitmann et al., 2003). (g) Three-point running average of *G. ruber* $\delta^{18}O$ in in the PS009PC core (Levantine Sea) (red line) (Hennekam et al., 2014). (h) K^+ record from the GISP2 Greenland ice core (black line) (Mayewski et al., 1997) (i) Stacked drift-ice records from four North Atlantic cores (black line) (Bond et al., 2001). Light gray vertical bands indicate the three 9.3–8.8, 8.5–7.8, and 7.3–6.8 ka perturbation intervals discussed in the text.

6.3. East Africa and Global Monsoon

In the previous section and in Figure 7, the Oman speleothem and the Gulf of Guinea Ba/Ca record are assumed as a proxy for monsoon activity. It is still unclear whether and to what extent the West African monsoon and the Indian monsoon contributed to river runoff into the eastern Mediterranean during sapropel deposition. Regional monsoons vary coherently at millennial and orbital scale with minor differences due to their own features (Wang et al., 2014). A considerable body of proxy records indicates that North Hemisphere summer monsoon systems, including North Africa, India, East Asia, and North America, abruptly weakened during Greenland stadials (Cheng et al., 2012; Wang et al., 2014). Also, there is evidence of coordinated changes between the eastern Mediterranean Sea, Indian, and Asian monsoons at orbital-scale and during the Holocene (Marino et al., 2009; Ziegler et al., 2010). In fact, the 9.2 ka event is relevant in the Asian Monsoon, where it is the strongest Holocene activity weakening (Zhang et al., 2018). The 8.2 ka event is widespread (Cheng et al., 2016; Dixit et al., 2014; Fleitmann et al., 2003; Wang et al., 2014).

The single contribution from different monsoon systems to the Nile River freshwater discharge during the early-middle Holocene has been evaluated by Hennekam et al. (2014). These authors concluded that there was a leading activity by the Indian monsoon, compared to the West African monsoon, during sapropel S1 deposition (Hennekam et al., 2014). However, at least for 9.2, 8.2, and 7.2 ka events, the activity weakening seems to be a common feature of both monsoon systems (Figures 7b and 7f).

In previous studies, the Soreq Cave (Israel) and Jeita Cave (Lebanon) speleothem $\delta^{18}O$ records have been associated to sapropels and to monsoon that fuels the Nile River catchment, but their isotopic source is from the Mediterranean Sea water evaporation (Bar-Matthews et al., 2000; Cheng et al., 2015; Rohling et al., 2019), even though it may have partially captured the monsoon signal from freshwater discharge into the Levantine Sea (Rohling et al., 2015; Wang et al., 2014). This may explain why the 9.2 and 7.2 ka events are not fully recorded in Israel and are recorded with minor timing differences in Lebanon. The Ba/Ca was considered another proxy for river runoff into the Mediterranean Sea (Sprovieri et al., 2008, 2012; Weldeab et al., 2007). In Core SL112, this ratio strongly supports the occurrence of a weakened monsoon activity at 9.2 ka, after the maximum Nile River flooding (Figure 6l), but fails to present millennial-scale variability that is evident in any monsoon record (Weldeab et al., 2014). However, millennial-scale variability of Nile River flooding and its decrease during 9.3–8.8, 8.5–7.8, and 7.3–6.8 ka time intervals are visible as heavier *G. ruber* $\delta^{18}O$ values in the Levantine Sea (Figure 7g) (Hennekam et al., 2014).

The weakened monsoon activity around 9.2, 8.2, and 7.2 ka may be explained by the reduced solar output, as inferred by $\Delta^{14}C$ residuals, Greenland ice cores ^{10}Be, and sunspot number reconstructions (Finkel & Nishiizumi, 1997; Solanki et al., 2004). The thermal contrast weakening between the continent and the ocean or between hemispheres would have reduced monsoon circulation and its precipitation (Wang et al., 2017; Yan et al., 2015). The subsequent southward shift of the intertropical convergence zone would have narrowed the Nile River catchment and decreased the freshwater discharge into the eastern Mediterranean (Hennekam et al., 2014; Rohling, Cane, et al., 2002; Wang et al., 2017). A very similar result for monsoon activity weakening around 9.2, 8.2, and 7.2 ka is also possibly explained by the Atlantic Meridional Overturning Circulation (AMOC) slowdown, a phenomenon which is well known during stadials and Heinrich events of the last glacial (Broccoli et al., 2006; Wang et al., 2005). However, changes in the AMOC strength during Holocene rapid climatic changes are not fully established (Mayewski et al., 2004).

6.4. Cold Polar/Continental Air Outbreaks and the Bernoulli Aspiration Effect

There are different mechanisms, other than monsoon activity, that may have driven denser LIW production and western Mediterranean seafloor oxygen advection. EMDW and LIW formation is promoted by cold polar/continental air outbreaks, whose frequency during the Holocene has been recently modeled for the Aegean Sea region (Rohling et al., 2019), establishing a tight relationship with the Greenland GISP2 K^+ record (Mayewski et al., 1997), a proxy for the Siberian High strength and rapid climatic changes (Mayewski et al., 2004; Rohling, Mayewski, et al., 2002). However, the Siberian High strengthening and the increased frequency of northerly air outbreaks, within the selected 10.0–6.5 ka time interval, may be limited to the 8.2 ka event and within age uncertainties to the 9.2 ka event (Figure 7h). This suggests the prominent role of monsoon weakening for the denser LIW and the increased zonal circulation observed in the Sicily Channel.

Also North Atlantic ice rafted detritus (IRD) episodes (Figure 7i) (Bond et al., 2001) are associated to Holocene rapid climatic changes and are thought to be the trigger of North Atlantic Oscillation positive-like conditions that stimulate WMDW production (Frigola et al., 2008; Incarbona et al., 2008). But even in this case, North Atlantic IRD peaks seem to be misaligned (slightly earlier) with respect to western Mediterranean bottom water circulation and ORL termination (Figures 7a, 7c, and 7D). Though once again the age uncertainty cannot conclusively rule out the North Atlantic Ocean influence, the significant and repeated misalignment would support the importance of LIW preconditioning.

The Bernoulli aspiration of old WMDW over the Gibraltar sill is an effective mechanism to bring oxygen on the seafloor, other than deep water formation. This process is essentially controlled by outflow water velocity and density difference across the sill (Rogerson, 2012; Rogerson et al., 2008; Rohling et al., 2015). From calculations, it was concluded that the ORL deposition interval may be explained by the interplay of sea level rise, Atlantic Ocean melt water events, freshwater discharge into the eastern Mediterranean, and alpine meltwater into the northwestern Mediterranean during the deglaciation (Rogerson et al., 2008; Rohling et al., 2015). This interaction was likely responsible for the ORL onset, and without the alpine meltwater perturbation in the western Mediterranean, sapropels and ORLs timing would be very similar (Rohling et al., 2015). In fact, LIW transports the salinity decrease of monsoon flooding and adversely affects WMDW production (Emeis et al., 1991; Rohling et al., 2015). Equally, we note that monsoon weakening may be responsible for a denser LIW that, once transferred to the western Mediterranean, may have promoted WMDW production and seafloor oxygenation, possibly interrupting the most recent ORL deposition.

7. Conclusion

Stable isotopic measurements were collected on three foraminifera species in the Sicily Channel ODP Hole 963D over the last 12.0 kyr. A total of 129 and 94 were, respectively, analyzed for *G. ruber* and *N. incompta* $\delta^{18}O$, 129 samples for *U. mediterranea* $\delta^{18}O$ and $\delta^{13}C$. The average sampling resolution is of 84 years for *G. ruber* and *U. mediterranea* and of 115 years for *N. incompta*.

LIW density and Sicily Channel seafloor ventilation seem to be modified with changing eastern Mediterranean sapropel S1 circumstances: LIW density decreases and reduced seafloor ventilation are recorded coinciding with the sapropel onset and the maximum Nile River flooding; the opposite scenario can be observed during sapropel interruption at 8.5–7.8 ka.

Sicily Channel isotopic records are compared with data from well-constrained eastern and western Mediterranean cores. Millennial-scale variability in the eastern Mediterranean (the end of maximum Nile River flooding at 9.2 ka, seafloor reventilation episodes in the Adriatic and Aegean Seas at 8.2 and 7.2 ka) seems to be driven by distinct phases of monsoon activity weakening. These phases can be summarized as 9.3–8.8, 8.5–7.8, and 7.3–6.8 ka events and can be observed in the Sicily Channel, through the passage of a denser LIW and higher seafloor ventilation. These events correspond with the final alkenone and TOC accumulation in the western Mediterranean that marks the ORL termination. The UP10 sortable silt record in the Balearic Sea indicates the concurrent recovery of sea bottom circulation. We conclude that monsoon weakening led to the production of denser LIW that was transmitted into the western basin and promoted WMDW formation and seafloor oxygenation. In other words, eastern Mediterranean perturbations during sapropel S1 deposition, due to monsoon weakening, were transmitted into the western Mediterranean through the zonal vertical circulation belt and contributed to exhaust organic-rich layers accumulation.

Data Availability Statement

The data set is available on the Pangaea repository.

Acknowledgments

We are grateful to Rick Hennekam and Gianluca Marino for their valuable comments and suggestions. This research was supported by the Italian Ministry of Education, Universities and Research, PJ_RIC_FFABR_2017_161560 and FFR_D14 grants to A. I.

References

Abu-Zied, R. H., Rohling, E. J., Jorissen, F. J., Fontanier, C., Casford, J. S. L., & Cooke, S. (2008). Benthic foraminiferal response to changes in bottom-water oxygenation and organic carbon flux in the eastern Mediterranean during LGM to Recent times. *Marine Micropaleontology*, *67*(1–2), 46–68. https://doi.org/10.1016/j.marmicro.2007.08.006

Amies, J. D., Rohling, E. J., Grant, K. M., Rodríguez-Sanz, L., & Marino, G. (2019). Quantification of African Monsoon runoff during Last Interglacial sapropel S5. *Paleoceanography and Paleoclimatology*, *34*(8), 1487–1516. https://doi.org/10.1029/2019PA003652

Bar-Matthews, M., Ayalon, A., & Kaufman, A. (2000). Timing and hydrological conditions of Sapropel events in the Eastern Mediterranean, as evident from speleothems, Soreq cave, Israel. *Chemical Geology*, *169*(1–2), 145–156. https://doi.org/10.1016/S0009-2541(99)00232-6

Bemis, B. E., Spero, H. J., Bijma, J., & Lea, D. W. (1998). Reevaluation of the oxygen isotopic composition of planktonic foraminifera: Experimental results and revised paleotemperature equations. *Paleoceanography*, *13*(2), 150–160. https://doi.org/10.1029/98PA00070

Bethoux, J. P., Gentili, B., Morin, P., Nicolas, E., Pierre, C., & Ruiz-Pino, D. (1999). The Mediterranean Sea: A miniature ocean for climatic and environmental studies and a key for the climatic functioning of the North Atlantic. *Progress in Oceanography*, *44*(1–3), 131–146. https://doi.org/10.1016/S0079-6611(99)00023-3

Bond, G., Kromer, B., Beer, J., Muscheler, R., Evans, M. N., Showers, W., et al. (2001). Persistent solar influence on North Atlantic climate during the Holocene. *Science*, *294*(5549), 2130–2136. https://doi.org/10.1126/science.1065680

Böttcher, M. E., Rinna, J., Warning, B., Wehausen, R., Howell, M. W., Schnetger, B., et al. (2003). Geochemistry of sediments from the connection between the western and the eastern Mediterranean Sea (Strait of Sicily, ODP Site 963). *Palaeogeography, Palaeoclimatology, Palaeoecology*, *190*, 165–194. https://doi.org/10.1016/S0031-0182(02)00604-1

Bout-Roumazeilles, V., Combourieu-Nebout, N., Desprat, S., Siani, G., Turon, J. L., & Essallami, L. (2013). Tracking atmospheric and riverine terrigenous supplies variability during the last glacial and the Holocene in central Mediterranean. *Climate of the Past*, *9*(3), 1065–1087. https://doi.org/10.5194/cp-9-1065-2013

Broccoli, A. J., Dahl, K. A., & Stouffer, R. J. (2006). Response of the ITCZ to Northern Hemisphere cooling. *Geophysical Research Letters*, *33*, L01702. https://doi.org/10.1029/2005GL024546

Cacho, I., Grimalt, J. O., & Canals, M. (2002). Response of the Western Mediterranean Sea to rapid climatic variability during the last 50,000 years: A molecular biomarker approach. *Journal of Marine Systems*, *33–34*, 253–272. https://doi.org/10.1016/S0924-7963(02)00061-1

Cacho, I., Grimalt, J. O., Pelejero, C., Canals, M., Sierro, F. J., Flores, J. A., & Shackleton, N. (1999). Dansgaard-Oeschger and Heinrich event imprints in Alboran Sea paleotemperatures. *Paleoceanography*, *14*(6), 698–705. https://doi.org/10.1029/1999PA900044

Cacho, I., Grimalt, J. O., Sierro, F. J., Shackleton, N., & Canals, M. (2000). Evidence for enhanced Mediterranean thermohaline circulation during rapid climatic coolings. *Earth and Planetary Science Letters*, *183*(3–4), 417–429. https://doi.org/10.1016/S0012-821X(00)00296-X

Casford, J. S. L., Rohling, E. J., Abu-Zied, R. H., Fontanier, C., Jorissen, F. J., Leng, M. J., et al. (2003). A dynamic concept for eastern Mediterranean circulation and oxygenation during sapropel formation. *Palaeogeography, Palaeoclimatology, Palaeoecology*, *190*, 103–119. https://doi.org/10.1016/S0031-0182(02)00601-6

Cheng, H., Edwards, R. L., Sinha, A., Spötl, C., Yi, L., Chen, S., et al. (2016). The Asian monsoon over the past 640,000 years and ice age terminations. *Nature*, *534*(7609), 640–646. https://doi.org/10.1038/nature18591

Cheng, H., Sinha, A., Verheyden, S., Nader, F. H., Li, X. L., Zhang, P. Z., et al. (2015). The climate variability in northern Levant over the past 20,000 years. *Geophysical Research Letters*, *42*, 8641–8650. https://doi.org/10.1002/2015GL065397

Cheng, H., Sinha, A., Wang, X., Cruz, F. W., & Edwards, R. L. (2012). The Global Paleomonsoon as seen through speleothem records from Asia and the Americas. *Climate Dynamics*, *39*(5), 1045–1062. https://doi.org/10.1007/s00382-012-1363-7

De Lange, G. J., Thomson, J., Reitz, A., Slomp, C. P., Principato, M. S., Erba, E., & Corselli, C. (2008). Synchronous basin-wide formation and redox-controlled preservation of a Mediterranean sapropel. *Nature Geoscience*, *1*, 606–610. https://doi.org/10.1038/ngeo283

De Rijk, S., Jorissen, F. J., Rohling, E. J., & Troelstra, S. R. (2000). Organic flux control on bathymetric zonation of Mediterranean benthic foraminifera. *Marine Micropaleontology*, *40*(3), 151–166. https://doi.org/10.1016/S0377-8398(00)00037-2

Di Donato, V., Insinga, D. D., Iorio, M., Molisso, F., Rumolo, P., Cardines, C., & Passaro, S. (2019). The palaeoclimatic and palaeoceanographic history of the Gulf of Taranto (Mediterranean Sea) in the last 15 ky. *Global and Planetary Change*, *172*, 278–297. https://doi.org/10.1016/j.gloplacha.2018.10.014

Dixit, Y., Hodell, D. A., Sinha, R., & Petrie, C. (2014). Abrupt weakening of the Indian summer monsoon at 8.2 kyr BP. *Earth and Planetary Science Letters*, *391*, 16–23. https://doi.org/10.1016/j.epsl.2014.01.026

Dubois-Dauphin, Q., Montagna, P., Siani, G., Douville, E., Wienberg, C., Hebbeln, D., et al. (2017). Hydrological variations of the intermediate water masses of the western Mediterranean Sea during the past 20 ka inferred from neodymium isotopic composition in foraminifera and cold-water corals. *Climate of the Past*, *13*(1), 17–37. https://doi.org/10.5194/cp-13-17-2017

Emeis, K.-C., Camerlenghi, A., McKenzie, J. A., Rio, D., & Sprovieri, R. (1991). The occurrence and significance of Pleistocene and Upper Pliocene sapropels in the Tyrrhenian Sea. *Marine Geology*, *100*(1), 155–182. https://doi.org/10.1016/0025-3227(91)90231-R

Emeis, K.-C., Robertson, A. H. F., Richter, C., & Shipboard party (1996). Site 963. In K.-C. Emeis, A. H. F. Robertson, & C. Richter (Eds.), *Proceedings of the Ocean Drilling Program, Initial Reports, Leg 160* (Vol. 160, pp. 55–84). College Station, TX: Ocean Drilling Program.

Emeis, K.-C., Schulz, H., Struck, U., Rossignol-Strick, M., Erlenkeuser, H., Howell, M. W., et al. (2003). Eastern Mediterranean surface water temperatures and δ^{18}O composition during deposition of sapropels in the late Quaternary. *Paleoceanography*, *18*(1), 1005. https://doi.org/10.1029/2000PA000617

Emeis, K. C., Struck, U., Schulz, H. M., Rosenberg, R., Bernasconi, S., Erlenkeuser, H., et al. (2000). Temperature and salinity variations of Mediterranean Sea surface waters over the last 16,000 years from records of planktonic stable oxygen isotopes and alkenone unsaturation ratios. *Palaeogeography, Palaeoclimatology, Palaeoecology*, *158*(3–4), 259–280. https://doi.org/10.1016/S0031-0182(00)00053-5

Fairbanks, R. G., & Wiebe, P. H. (1980). Foraminifera and chlorophyll maximum: Vertical distribution, seasonal succession, and paleoceanographic significance. *Science*, *209*, 1524–1526.

Filippidi, A., & De Lange, G. J. (2019). Eastern Mediterranean deep water formation during sapropel S1: A reconstruction using geochemical records along a bathymetric transect in the Adriatic Outflow Region. *Paleoceanography and Paleoclimatology*, *34*(3), 409–429. https://doi.org/10.1029/2018PA003459

Filippidi, A., Triantaphyllou, M. V., & De Lange, G. J. (2016). Eastern-Mediterranean ventilation variability during sapropel S1 formation, evaluated at two sites influenced by deep-water formation from Adriatic and Aegean Seas. *Quaternary Science Reviews*, *144*, 95–106. https://doi.org/10.1016/j.quascirev.2016.05.024

Finkel, R. C., & Nishiizumi, K. (1997). Beryllium 10 concentrations in the Greenland Ice Sheet Project 2 ice core from 3–40 ka. *Journal of Geophysical Research*, *102*(C12), 26,699–26,706. https://doi.org/10.1029/97JC01282

Fleitmann, D., Burns, S. J., Mudelsee, M., Neff, U., Kramers, J., Mangini, A., & Matter, A. (2003). Holocene Forcing of the Indian Monsoon Recorded in a Stalagmite from Southern Oman. *Science*, *300*(5626), 1737–1739. https://doi.org/10.1126/science.1083130

Fontanier, C., Jorissen, F. J., Lansard, B., Mouret, A., Buscail, R., Schmidt, S., et al. (2008). Live foraminifera from the open slope between Grand Rhône and Petit Rhône Canyons (Gulf of Lions, NW Mediterranean). *Deep Sea Research Part I: Oceanographic Research Papers*, *55*(11), 1532–1553. https://doi.org/10.1016/j.dsr.2008.07.003

Fontanier, C., Mackensen, A., Jorissen, F. J., Anschutz, P., Licari, L., & Griveaud, C. (2006). Stable oxygen and carbon isotopes of live benthic foraminifera from the Bay of Biscay: Microhabitat impact and seasonal variability. *Marine Micropaleontology*, *58*(3), 159–183. https://doi.org/10.1016/j.marmicro.2005.09.004

Frigola, J., Moreno, A., Cacho, I., Canals, M., Sierro, F. J., Flores, J. A., & Grimalt, J. O. (2008). Evidence of abrupt changes in Western Mediterranean Deep Water circulation during the last 50 kyr: A high-resolution marine record from the Balearic Sea. *Quaternary International*, *181*(1), 88–104. https://doi.org/10.1016/j.quaint.2007.06.016

Gasparini, G. P., Ortona, A., Budillon, G., Astraldi, M., & Sansone, E. (2005). The effect of the Eastern Mediterranean Transient on the hydrographic characteristics in the Strait of Sicily and in the Tyrrhenian Sea. *Deep Sea Research Part I: Oceanographic Research Papers*, *52*(6), 915–935. https://doi.org/10.1016/j.dsr.2005.01.001

Grant, K. M., Rohling, E. J., Bar-Matthews, M., Ayalon, A., Medina-Elizalde, M., Ramsey, C. B., et al. (2012). Rapid coupling between ice volume and polar temperature over the past 50,000 years. *Nature*, *491*(7426), 744–747. https://doi.org/10.1038/nature11593

Grimm, R., Maier-Reimer, E., Mikolajewicz, U., Schmiedl, G., Müller-Navarra, K., Adloff, F., et al. (2015). Late glacial initiation of Holocene eastern Mediterranean sapropel formation. *Nature Communications*, *6*, 7099. https://doi.org/10.1038/ncomms8099

Hall, I. R., McCave, I. N., Shackleton, N. J., Weedon, G. P., & Harris, S. E. (2001). Intensified deep Pacific inflow and ventilation in Pleistocene glacial times. *Nature*, *412*(6849), 809–812. https://doi.org/10.1038/35090552

Hemleben, C., Spindler, M., & Anderson, O. R. (1989). In Springer (Ed.), *Modern planktonic foraminifera*. Berlin, Heidelberg: Springer-Verlag.

Hennekam, R., Jilbert, T., Schnetger, B., & de Lange, G. J. (2014). Solar forcing of Nile discharge and sapropel S1 formation in the early to middle Holocene eastern Mediterranean. *Paleoceanography*, *29*, 343–356. https://doi.org/10.1002/2013PA002553

Hernández-Almeida, I., Bárcena, M. A., Flores, J. A., Sierro, F. J., Sanchez-Vidal, A., & Calafat, A. (2011). Microplankton response to environmental conditions in the Alboran Sea (Western Mediterranean): One year sediment trap record. *Marine Micropaleontology*, *78*(1–2), 14–24. https://doi.org/10.1016/j.marmicro.2010.09.005

Hilgen, F. J. (1991). Astronomical calibration of Gauss to Matuyama sapropels in the Mediterranean and implication for the Geomagnetic Polarity Time Scale. *Earth and Planetary Science Letters*, *104*(2–4), 226–244. https://doi.org/10.1016/0012-821x(91)90206-w

Hodell, D. A., Nicholl, J. A., Bontognali, T. R. R., Danino, S., Dorador, J., Dowdeswell, J. A., et al. (2017). Anatomy of Heinrich Layer 1 and its role in the last deglaciation. *Paleoceanography*, *32*, 284–303. https://doi.org/10.1002/2016PA003028

Incarbona, A., Abu-Zied, R. H., Rohling, E. J., & Ziveri, P. (2019). Reventilation episodes during the sapropel S1 deposition in the Eastern Mediterranean based on holococcolith preservation. *Paleoceanography and Paleoclimatology*, *34*(10), 1597–1609. https://doi.org/10.1029/2019PA003626

Incarbona, A., Di Stefano, E., Parti, B., Pelosi, N., Bonomo, S., Mazzola, S., et al. (2008). Holocene millennial-scale productivity variations in the Sicily Channel (Mediterranean Sea). *Paleoceanography*, *23*, PA3204. https://doi.org/10.1029/2007PA001581

Incarbona, A., Jonkers, L., Ferraro, S., Sprovieri, R., & Tranchida, G. (2019). Sea surface temperatures and paleoenvironmental variability in the central Mediterranean during historical times reconstructed using planktonic foraminifera. *Paleoceanography and Paleoclimatology*, *34*(3), 394–408. https://doi.org/10.1029/2018PA003529

Incarbona, A., Martrat, B., Mortyn, P. G., Sprovieri, M., Ziveri, P., Gogou, A., et al. (2016). Mediterranean circulation perturbations over the last five centuries: Relevance to past Eastern Mediterranean Transient-type events. *Scientific Reports*, *6*(1), 29623. https://doi.org/10.1038/srep29623

Incarbona, A., Sprovieri, M., Di Stefano, A., Di Stefano, E., Salvagio Manta, D., Pelosi, N., et al. (2013). Productivity modes in the mediterranean sea during dansgaard-oeschger (20,000–70,000 yr ago) oscillations. *Palaeogeography, Palaeoclimatology, Palaeoecology*, *392*, 128–137. https://doi.org/10.1016/j.palaeo.2013.09.023

Jimenez-Espejo, F. J., Martinez-Ruiz, F., Rogerson, M., González-Donoso, J. M., Romero, O. E., Linares, D., et al. (2008). Detrital input, productivity fluctuations, and water mass circulation in the westernmost Mediterranean Sea since the Last Glacial Maximum. *Geochemistry, Geophysics, Geosystems*, *9*, Q11U02. https://doi.org/10.1029/2008GC002096

Jimenez-Espejo, F. J., Martinez-Ruiz, F., Sakamoto, T., Iijima, K., Gallego-Torres, D., & Harada, N. (2007). Paleoenvironmental changes in the western Mediterranean since the last glacial maximum: High resolution multiproxy record from the Algero-Balearic basin. *Palaeogeography, Palaeoclimatology, Palaeoecology*, *246*(2–4), 292–306. https://doi.org/10.1016/j.palaeo.2006.10.005

Jorissen, F. J. (1999). Benthic foraminiferal successions across Late Quaternary Mediterranean sapropels. *Marine Geology*, *153*, 91–101.

Knappertsbusch, M. (1993). Geographic distribution of living and Holocene coccolithophores in the Mediterranean Sea. *Marine Micropaleontology*, *21*(1–3), 219–247. https://doi.org/10.1016/0377-8398(93)90016-Q

Kuhnt, T., Schmiedl, G., Ehrmann, W., Hamann, Y., & Hemleben, C. (2007). Deep-sea ecosystem variability of the Aegean Sea during the past 22 kyr as revealed by Benthic Foraminifera. *Marine Micropaleontology*, *64*(3), 141–162. https://doi.org/10.1016/j.marmicro.2007.04.003

Lambeck, K., Rouby, H., Purcell, A., Sun, Y., & Sambridge, M. (2014). Sea level and global ice volumes from the Last Glacial Maximum to the Holocene. *Proceedings of the National Academy of Sciences*, *111*(43), 15,296–15,303. https://doi.org/10.1073/pnas.1411762111

Le Houedec, S., Mojtahid, M., Bicchi, E., de Lange, G. J., & Hennekam, R. (2020). Suborbital hydrological variability inferred from coupled benthic and planktic foraminiferal-based proxies in the southeastern Mediterranean during the last 19 ka. *Paleoceanography and Paleoclimatology*, *35*(2), e2019PA003827. https://doi.org/10.1029/2019PA003827

LeGrande, A. N., & Schmidt, G. A. (2006). Global gridded data set of the oxygen isotopic composition in seawater. *Geophysical Research Letters*, *33*, L12604. https://doi.org/10.1029/2006GL026011

Lermusiaux, P. F. J., & Robinson, A. R. (2001). Features of dominant mesoscale variability, circulation patterns and dynamics in the strait of sicily. *Deep Sea Research Part I: Oceanographic Research Papers*, *48*(9), 1953–1997. https://doi.org/10.1016/S0967-0637(00)00114-X

Lourens, L. J., Antonarakou, A., Hilgen, F. J., Van Hoof, A. A. M., Vergnaud-Grazzini, C., & Zachariasse, W. J. (1997). Evaluation of the Plio-Pleistocene astronomical timescale. *Paleoceanography*, *12*(3), 527. https://doi.org/10.1029/97PA00321

Mackensen, A., Hubberten, H.-W., Bickert, T., Fischer, G., & Fütterer, D. K. (1993). The δ13C in benthic foraminiferal tests of Fontbotia wuellerstorfi (Schwager) Relative to the δ13C of dissolved inorganic carbon in Southern Ocean Deep Water: Implications for glacial ocean circulation models. *Paleoceanography*, *8*(5), 587–610. https://doi.org/10.1029/93PA01291

Magny, M., Vannière, B., Calo, C., Millet, L., Leroux, A., Peyron, O., et al. (2011). Holocene hydrological changes in south-western Mediterranean as recorded by lake-level fluctuations at Lago Preola, a coastal lake in southern Sicily, Italy. *Quaternary Science Reviews*, *30*(19–20), 2459–2475. https://doi.org/10.1016/j.quascirev.2011.05.018

Maiorano, P., Marino, M., & De Lange, G. J. (2019). Dynamic surface-water alterations during sapropel S1 preserved in high-resolution shallow-water sediments of Taranto Gulf, central Mediterranean. *Palaeogeography, Palaeoclimatology, Palaeoecology*, *534*, 109340. https://doi.org/10.1016/j.palaeo.2019.109340

Malanotte-Rizzoli, P., Artale, V., Borzelli-Eusebi, G. L., Brenner, S., Crise, A., Gacic, M., et al. (2014). Physical forcing and physical/biochemical variability of the Mediterranean Sea: A review of unresolved issues and directions for future research. *Ocean Science*, *10*(3), 281–322. https://doi.org/10.5194/os-10-281-2014

Malanotte-Rizzoli, P., & Hecht, A. (1988). Large-scale properties of the eastern Mediterranean: A review. *Oceanologica Acta*, *11*(4), 323–335. https://doi.org/10.1016/S0967-0645(99)00020-X

Marino, G., Rohling, E. J., Sangiorgi, F., Hayes, A., Casford, J. L., Lotter, A. F., et al. (2009). Early and middle Holocene in the Aegean Sea: Interplay between high and low latitude climate variability. *Quaternary Science Reviews*, *28*(27–28), 3246–3262. https://doi.org/10.1016/j.quascirev.2009.08.011

Martrat, B., Grimalt, J. O., Lopez-Martinez, C., Cacho, I., Sierro, F. J., Flores, J. A., et al. (2004). Abrupt temperature changes in the Western Mediterranean over the past 250,000 years. *Science*, *306*(5702), 1762–1765. https://doi.org/10.1126/science.1101706

Martrat, B., Jimenez-Amat, P., Zahn, R., & Grimalt, J. O. (2014). Similarities and dissimilarities between the last two deglaciations and interglaciations in the North Atlantic region. *Quaternary Science Reviews*, *99*, 122–134. https://doi.org/10.1016/j.quascirev.2014.06.016

Mayewski, P. A., Meeker, L. D., Twickler, M. S., Whitlow, S., Yang, Q., Lyons, W. B., & Prentice, M. (1997). Major features and forcing of high-latitude northern hemisphere atmospheric circulation using a 110,000-year-long glaciochemical series. *Journal of Geophysical Research*, *102*(C12), 26,345–26,366. https://doi.org/10.1029/96JC03365

Mayewski, P. A., Rohling, E. E., Curt Stager, J., Karlén, W., Maasch, K. A., Meeker, L. D., et al. (2004). Holocene climate variability. *Quaternary Research*, *62*(3), 243–255. https://doi.org/10.1016/j.yqres.2004.07.001

McCorkle, D. C., & Emerson, S. R. (1988). The relationship between pore water carbon isotopic composition and bottom water oxygen concentration. *Geochimica et Cosmochimica Acta*, *52*(5), 1169–1178. https://doi.org/10.1016/0016-7037(88)90270-0

Millot, C. (1999). Circulation in the Western Mediterranean Sea. *Journal of Marine Systems*, *20*(1–4), 423–442. https://doi.org/10.1016/S0924-7963(98)00078-5

Myers, P. G., Haines, K., & Rohling, E. J. (1998). Modeling the paleocirculation of the Mediterranean: The last glacial maximum and the Holocene with emphasis on the formation of sapropel S1. *Paleoceanography*, *13*(6), 586–606.

Pérez-Asensio, J. N., Frigola, J., Pena, L. D., Sierro, F. J., Reguera, M. I., Rodríguez-Tovar, F. J., et al. (2020). Changes in western Mediterranean thermohaline circulation in association with a deglacial Organic Rich Layer formation in the Alboran Sea. *Quaternary Science Reviews*, *228*, 106075. https://doi.org/10.1016/j.quascirev.2019.106075

Pinardi, N., & Masetti, E. (2000). Variability of the large scale general circulation of the Mediterranean Sea from observations and modelling: A review. *Palaeogeography, Palaeoclimatology, Palaeoecology*, *158*(3–4), 153–173. https://doi.org/10.1016/S0031-0182(00)00048-1

Pujol, C., & Grazzini, C. V. (1995). Distribution patterns of live planktic foraminifera as related to regional hydrography and productive system of the Mediterranean Sea. *Marine Micropaleontology*, *25*, 187–217.

Ramsey, C. B. (2008). Deposition models for chronological records. *Quaternary Science Reviews*, *27*(1), 42–60. https://doi.org/10.1016/j.quascirev.2007.01.019

Reimer, P. J., Bard, E., Bayliss, A., Beck, J. W., Blackwell, P. G., Ramsey, C. B., et al. (2013). IntCal13 and Marine13 radiocarbon age calibration curves 0–50,000 years cal BP. *Radiocarbon*, *55*(4), 1869–1887. https://doi.org/10.2458/azu_js_rc.55.16947

Rigual-Hernández, A. S., Sierro, F. J., Bárcena, M. A., Flores, J. A., & Heussner, S. (2012). Seasonal and interannual changes of planktic foraminiferal fluxes in the Gulf of Lions (NW Mediterranean) and their implications for paleoceanographic studies: Two 12-year sediment trap records. *Deep Sea Research Part I: Oceanographic Research Papers*, *66*, 26–40. https://doi.org/10.1016/j.dsr.2012.03.011

Robinson, A. R., & Golnaraghi, M. (1994). The physical and dynamical oceanography of the Mediterranean Sea. In *Ocean Processes in Climate Dynamics: Global and Mediterranean Examples*, *NATO ASI Series* (Vol. 419, pp. 255–306). https://link.springer.com/chapter/10.1007/978-94-011-0870-6_12

Rodríguez-Sanz, L., Bernasconi, S. M., Marino, G., Heslop, D., Müller, I. A., Fernandez, A., et al. (2017). Penultimate deglacial warming across the Mediterranean Sea revealed by clumped isotopes in foraminifera. *Scientific Reports*, *7*(1), 16572. https://doi.org/10.1038/s41598-017-16528-6

Roether, W., Manca, B. B., Klein, B., Bregant, D., Georgopoulos, D., Beitzel, V., et al. (1996). Recent changes in eastern Mediterranean deep waters. *Science*, *271*(5247), 333–335. https://doi.org/10.1126/science.271.5247.333

Rogerson, E. J. R. (2012). Paleoceanography of the Atlantic-Mediterranean exchange: Overview and first quantitative assessment of climatic forcing. *Reviews of Geophysics*, *50*, RG2003. https://doi.org/10.1029/2011RG000376

Rogerson, M., Cacho, I., Jimenez-Espejo, F., Reguera, M. I., Sierro, F. J., Martinez-Ruiz, F., et al. (2008). A dynamic explanation for the origin of the western Mediterranean organic-rich layers. *Geochemistry, Geophysics, Geosystems*, *9*, Q07U01. https://doi.org/10.1029/2007GC001936

Rohling, E. J., & Bigg, G. R. (1998). Paleosalinity and delta-8O: A critical assessment. *Journal of Geophysical Research*, *103*(C1), 1307–1318. https://doi.org/10.1029/97JC01047

Rohling, E. J., Cane, T. R., Cooke, S., Sprovieri, M., Bouloubassi, I., Emeis, K. C., et al. (2002). African monsoon variability during the previous interglacial maximum. *Earth and Planetary Science Letters*, *202*(1), 61–75. https://doi.org/10.1016/S0012-821X(02)00775-6

Rohling, E. J., Foster, G. L., Grant, K. M., Marino, G., Roberts, A. P., Tamisiea, M. E., & Williams, F. (2014). Sea-level and deep-sea-temperature variability over the past 5.3 million years. *Nature*, *508*(7497), 477–482. https://doi.org/10.1038/nature13230

Rohling, E. J., & Gieskes, W. W. (1989). Late Quaternary changes in Mediterranean intermediate water density and formaton rate. *Paleoceanography*, *4*(5), 531–545.

Rohling, E. J., Marino, G., & Grant, K. M. (2015). Mediterranean climate and oceanography, and the periodic development of anoxic events (sapropels). *Earth-Science Reviews*, *143*. https://doi.org/10.1016/j.earscirev.2015.01.008

Rohling, E. J., Marino, G., Grant, K. M., Mayewski, P. A., & Weninger, B. (2019). A model for archaeologically relevant Holocene climate impacts in the Aegean-Levantine region (easternmost Mediterranean). *Quaternary Science Reviews*, *208*, 38–53. https://doi.org/10.1016/j.quascirev.2019.02.009

Rohling, E. J., Mayewski, P., Abu-Zied, R., Casford, J., & Hayes, A. (2002). Holocene atmosphere–ocean interactions: Records from Greenland and the Aegean sea. *Climate Dynamics*, *18*(7), 587–594. https://doi.org/10.1007/s00382-001-0194-8

Rohling, E. J., Sprovieri, M., Cane, T., Casford, J. S. L., Cooke, S., Bouloubassi, I., et al. (2004). Reconstructing past planktic foraminiferal habitats using stable isotope data: A case history for Mediterranean sapropel S5. *Marine Micropaleontology*, *50*(1–2), 89–123. https://doi.org/10.1016/S0377-8398(03)00068-9

Rossignol-Strick, M., Nesteroff, W., Olive, P., & Vergnaud-Grazzini, C. (1982). After the deluge: Mediterranean stagnation and sapropel formation. *Nature*, *295*, 105.

Schmiedl, G., De Bovée, F., Buscail, R., Charrière, B., Hemleben, C., Medernach, L., & Picon, P. (2000). Trophic control of benthic foraminiferal abundance and microhabitat in the bathyal Gulf of Lions, western Mediterranean Sea. *Marine Micropaleontology*, *40*(3), 167–188. https://doi.org/10.1016/S0377-8398(00)00038-4

Schmiedl, G., Pfeilsticker, M., Hemleben, C., & Mackensen, A. (2004). Environmental and biological effects on the stable isotope composition of recent deep-sea benthic foraminifera from the western Mediterranean Sea. *Marine Micropaleontology*, *51*(1–2), 129–152. https://doi.org/10.1016/j.marmicro.2003.10.001

Schönfeld, J., & Zahn, R. (2000). Late Glacial to Holocene history of the Mediterranean outflow. Evidence from benthic foraminiferal assemblages and stable isotopes at the Portuguese margin. *Palaeogeography, Palaeoclimatology, Palaeoecology*, *159*(1–2), 85–111. https://doi.org/10.1016/S0031-0182(00)00035-3

Schroeder, K., Josey, S. A., Herrmann, M., Grignon, L., Gasparini, G. P., & Bryden, H. L. (2010). Abrupt warming and salting of the Western Mediterranean Deep Water after 2005: Atmospheric forcings and lateral advection. *Journal of Geophysical Research*, *115*, C08029. https://doi.org/10.1029/2009JC005749

Schroeder, K., Ribotti, A., Borghini, M., Sorgente, R., Perilli, A., & Gasparini, G. P. (2008). An extensive western Mediterranean deep water renewal between 2004 and 2006. *Geophysical Research Letters*, *35*, L18605. https://doi.org/10.1029/2008GL035146

Sha, L., Ait Brahim, Y., Wassenburg, J. A., Yin, J., Peros, M., Cruz, F. W., et al. (2019). How far north did the African Monsoon fringe expand during the African humid period? Insights from southwest Moroccan speleothems. *Geophysical Research Letters*, *46*, 14,093–14,102. https://doi.org/10.1029/2019GL084879

Siani, G., Paterne, M., Arnold, M., Bard, E., Métivier, B., Tisnerat, N., & Bassinot, F. (2000). Radiocarbon reservoir ages in the Mediterranean Sea and Black Sea. *Radiocarbon*, *42*(2), 271–280. https://doi.org/10.1017/S0033822200059075

Sicre, M. A., Siani, G., Genty, D., Kallel, N., & Essallami, L. (2013). Seemingly divergent sea surface temperature proxy records in the central Mediterranean during the last deglaciation. *Climate of the Past*, *9*(3), 1375–1383. https://doi.org/10.5194/cp-9-1375-2013

Sierro, F. J., Hodell, D. A., Curtis, J. H., Flores, J. A., Reguera, I., Colmenero-Hidalgo, E., et al. (2005). Impact of iceberg melting on Mediterranean thermohaline circulation during Heinrich events. *Paleoceanography*, *20*, PA2019. https://doi.org/10.1029/2004PA001051

Skliris, N., & Lascaratos, A. (2004). Impacts of the Nile River damming on the thermohaline circulation and water mass characteristics of the Mediterranean Sea. *Journal of Marine Systems*, *52*(1), 121–143. https://doi.org/10.1016/j.jmarsys.2004.02.005

Solanki, S. K., Usoskin, I. G., Kromer, B., Schüssler, M., & Beer, J. (2004). Unusual activity of the Sun during recent decades compared to the previous 11,000 years. *Nature*, *431*(7012), 1084–1087. https://doi.org/10.1038/nature02995

Sprovieri, M., d'Alcalà, M. R., Manta, D. S., Bellanca, A., Neri, R., Lirer, F., et al. (2008). Ba/Ca evolution in water masses of the Mediterranean late Neogene. *Paleoceanography*, *23*, PA3205. https://doi.org/10.1029/2007PA001469

Sprovieri, M., Di Stefano, E., Incarbona, A., Salvagio Manta, D., Pelosi, N., Ribera d'Alcalà, M., & Sprovieri, R. (2012). Centennial- to millennial-scale climate oscillations in the Central-Eastern Mediterranean Sea between 20,000 and 70,000 years ago: Evidence from a high-resolution geochemical and micropaleontological record. *Quaternary Science Reviews*, *46*, 126–135. https://doi.org/10.1016/j.quascirev.2012.05.005

Stern, J. V., & Lisiecki, L. E. (2014). Termination 1 timing in radiocarbon-dated regional benthic δ18O stacks. *Paleoceanography*, *29*, 1127–1142. https://doi.org/10.1002/2014PA002700

Tamburrino, S., Insinga, D. D., Sprovieri, M., Petrosino, P., Tiepolo, M., Ii, F., & Universita, T. (2012). Major and trace element characterization of tephra layers offshore Pantelleria Island: insights into the last 200 ka of volcanic activity and contribution to the Mediterranean tephrochronology. *Journal of Quaternary Science*, *27*, 129–140. https://doi.org/10.1002/jqs.1504

Theodor, M., Schmiedl, G., Jorissen, F., & Mackensen, A. (2016). Stable carbon isotope gradients in benthic foraminifera as proxy for organic carbon fluxes in the Mediterranean Sea. *Biogeosciences*, *13*(23), 6385–6404. https://doi.org/10.5194/bg-13-6385-2016

Theodor, M., Schmiedl, G., & Mackensen, A. (2016). Stable isotope composition of deep-sea benthic foraminifera under contrasting trophic conditions in the western Mediterranean Sea. *Marine Micropaleontology*, *124*, 16–28. https://doi.org/10.1016/j.marmicro.2016.02.001

Toucanne, S., Angue Minto'o, C. M., Fontanier, C., Bassetti, M. A., Jorry, S. J., & Jouet, G. (2015). Tracking rainfall in the northern Mediterranean borderlands during sapropel deposition. *Quaternary Science Reviews*, *129*, 178–195. https://doi.org/10.1016/j.quascirev.2015.10.016

Toucanne, S., Jouet, G., Ducassou, E., Bassetti, M. A., Dennielou, B., Angue Minto'o, C. M., et al. (2012). A 130,000-year record of Levantine Intermediate Water flow variability in the Corsica Trough, western Mediterranean Sea. *Quaternary Science Reviews*, *33*, 55–73. https://doi.org/10.1016/j.quascirev.2011.11.020

Vadsaria, T., Ramstein, G., Dutay, J.-C., Li, L., Ayache, M., & Richon, C. (2019). Simulating the occurrence of the last sapropel event (S1): Mediterranean basin ocean dynamics simulations using Nd isotopic composition modeling. *Paleoceanography and Paleoclimatology*, *34*(2), 237–251. https://doi.org/10.1029/2019PA003566

Wagner, B., Vogel, H., Francke, A., Friedrich, T., Donders, T., Lacey, J. H., et al. (2019). Mediterranean winter rainfall in phase with African monsoons during the past 1.36 million years. *Nature*, *573*(7773), 256–260. https://doi.org/10.1038/s41586-019-1529-0

Wang, P. X., Wang, B., Cheng, H., Fasullo, J., Guo, Z., Kiefer, T., & Liu, Z. (2017). The global monsoon across time scales: Mechanisms and outstanding issues. *Earth-Science Reviews*, *174*, 84–121. https://doi.org/10.1016/j.earscirev.2017.07.006

Wang, P. X., Wang, B., Cheng, H., Fasullo, J., Guo, Z. T., Kiefer, T., & Liu, Z. Y. (2014). The global monsoon across timescales: Coherent variability of regional monsoons. *Climate of the Past*, *10*(6), 2007–2052. https://doi.org/10.5194/cp-10-2007-2014

Wang, Y., Cheng, H., Edwards, R. L., He, Y., Kong, X., An, Z., et al. (2005). The Holocene Asian Monsoon: Links to solar changes and North Atlantic climate. *Science*, *308*(5723), 854–857. https://doi.org/10.1126/science.1106296

Weldeab, S., Lea, D. W., Schneider, R. R., & Andersen, N. (2007). 155,000 years of West African monsoon and ocean thermal evolution. *Science*, *316*(5829), 1303–LP-1307. https://doi.org/10.1126/science.1140461

Weldeab, S., Menke, V., & Schmiedl, G. (2014). The pace of East African monsson evolution during the Holocene. *Geophysical Research Letters*, *41*, 1724–1731. https://doi.org/10.1002/2014GL059361

Wu, J., Pahnke, K., Böning, P., Wu, L., Michard, A., & de Lange, G. J. (2019). Divergent Mediterranean seawater circulation during Holocene sapropel formation—Reconstructed using Nd isotopes in fish debris and foraminifera. *Earth and Planetary Science Letters*, *511*, 141–153. https://doi.org/10.1016/j.epsl.2019.01.036

Wu, P., & Haines, K. (1996). Modeling the dispersal of Levantine Intermediate Water and its role in Mediterranean deep water formation. *Journal of Geophysical Research*, *101*(C3), 6591–6607. https://doi.org/10.1029/95JC03555

Yan, H., Wei, W., Soon, W., An, Z., Zhou, W., Liu, Z., et al. (2015). Dynamics of the intertropical convergence zone over the western Pacific during the Little Ice Age. *Nature Geoscience*, *8*, 315.

Zahn, R., Sarnthein, M., & Erlenkeuser, H. (1987). Benthic isotope evidence for changes of the Mediterranean outflow during the Late Quaternary. *Paleoceanography*, *2*(6), 543–559. https://doi.org/10.1029/PA002i006p00543

Žarić, S., Donner, B., Fischer, G., Mulitza, S., & Wefer, G. (2005). Sensitivity of planktic foraminifera to sea surface temperature and export production as derived from sediment trap data. *Marine Micropaleontology*, *55*(1–2), 75–105. https://doi.org/10.1016/j.marmicro.2005.01.002

Zhang, W., Yan, H., Dodson, J., Cheng, P., Liu, C., Li, J., et al. (2018). The 9.2 ka event in Asian summer monsoon area: the strongest millennial scale collapse of the monsoon during the Holocene. *Climate Dynamics*, *50*(7), 2767–2782. https://doi.org/10.1007/s00382-017-3770-2

Ziegler, M., Lourens, L. J., Tuenter, E., Hilgen, F., Reichart, G.-J., & Weber, N. (2010). Precession phasing offset between Indian summer monsoon and Arabian Sea productivity linked to changes in Atlantic overturning circulation. *Paleoceanography*, *25*, PA3213. https://doi.org/10.1029/2009PA001884

Zirks, E., Krom, M. D., Zhu, D., Schmiedl, G., & Goodman-Tchernov, B. N. (2019). Evidence for the presence of oxygen-depleted sapropel intermediate water across the eastern Mediterranean during sapropel S1. *ACS Earth and Space Chemistry*, *3*(10), 2287–2297. https://doi.org/10.1021/acsearthspacechem.9b00128

Ziveri, P., Rutten, A., De Lange, G. J., Thomson, J., & Corselli, C. (2000). Present-day coccolith fluxes recorded in central eastern Mediterranean sediment traps and surface sediments. *Palaeogeography, Palaeoclimatology, Palaeoecology*, *158*(3–4), 175–195. https://doi.org/10.1016/S0031-0182(00)00049-3